DNA Origami and Rheology

Presented in fulfillment of requirements for graduation with Honors Undergraduate Research Distinction in Chemical and Biomolecular Engineering at The Ohio State University

Submitted by: Patrick Kinnunen

Fall 2016

Faculty Advisor: Dr. Carlos Castro, Department of Mechanical and Aerospace Engineering

Graduate Advisor: Josh Johnson, Biophysics Graduate Program

Thesis Committee: Dr. Carlos Castro and Dr. Kurt Koelling, Department of Chemical and Biomolecular Engineering

Abstract

The macro-scale behavior of engineering and biological materials is governed by the composition of the constituent molecules. Therefore, understanding connections between behaviors at different scales is of vital importance for understanding complex materials such as polymer solutions, human tissue, or cellular cytoplasm. DNA origami, a technique which uses complementary base pairing of deoxyribonucleic acid (DNA) molecules to build nanostructures with unprecedented spatial precision, involves the combination of dozens of polymer molecules. In this work, the connection between DNA origami, rheology, and material structure will be explored. Specifically, this thesis will work towards two goals: Connecting the physical properties of DNA with the DNA origami folding process, and using a DNA origami nanosensor to measure properties of the microenvironment. A two state DNA origami sensor, called the Nanodyn, was designed which can change shape based on the presence of molecular crowding agents in solution. The dynamics of the Nanodyn were measured in solutions with varying weight percentages of polyethylene glycol (PEG) and it was shown that molecular crowding in solution can be measured using a fluorescent assay. Full characterization of the Nanodyn will allow for the *in situ* measurement of of biological materials. It also demonstrates the ability for DNA origami to study rheological behavior. We also aimed to establish methods to study the viscoelastic properties of DNA origami solutions. DNA origami structures are formed from hundreds of polymeric molecules, giving rise to potentially complex rheological behaviors that could vary through the course of self-assembly. As a foundation for studying complex DNA origami solutions, two techniques, bulk rheology and microrheology, were applied to study simpler solutions containing DNA. Bulk rheology showed that DNA has viscoelastic properties at concentrations relevant to DNA origami. However, the required sample size makes it incompatible with current scales of DNA origami production. Microrheology allowed for the measurement of solution viscosity and the microliter volume requirements make it highly amenable

for DNA origami, but methods need to be improved before they can be applied to quantitatively study to DNA origami solution properties or self-assembly.

Acknowledgements

Firstly, I would like to thank Dr. Carlos Castro for his mentorship and encouragement over the last two and a half years. From OhioMOD to the work presented here, His instruction and vision have been imperative to my development as a scientist.

I would also like to thank Josh Johnson. He was crucial for the completion of this thesis, from helping me with lab technique to the writing and editing of this document. More importantly, his unending curiosity and dedication to discovery are a constant inspiration.

I would also like to acknowledge the contributions from the Koelling lab. Thanks to Dr. Koelling for agreeing to serve on my thesis committee, and for allowing me to use the equipment in your lab. I would also like to thank Varun Venoor for his instruction on the use of the rheometer.

None of this would have been possible without the whole lab – the atmosphere in NBL is incredible. Specifically, I would like to thank Jenny Le for her help with my thesis proposal and thesis. Dr. Mike Hudoba invented the Nanodyn, a major part of this work. Kelly Kolotka and Sarah Bushman helped collect data for the Nanodyn chapter. Their diligence and hard work are appreciated, but not as much as their company. Finally, Amjad Akif has been the source of many stimulating discussions, and I have tried to approach research the same way he does since we started in OhioMOD together.

Lastly, I have to thank my family and friends. They kept me mostly sane for three years, to their unending credit.

Contents

Abstract 2
List of Tables and Figures 7
Chapter 1: Introduction – DNA and Viscoelasticity 9
Background 9
DNA Origami 9
Rheology 16
Molecular Crowding: 22
Significance: 24
Objective: 25
Chapter 2: Molecular Crowding and DNA Origami 27
Introduction 27
Background 27
The Nanodyn: 27
Förster Resonance Energy Transfer 29
Methods 31
Structure Folding and Validation 31
Fluorescence Measurements 33
Results 34
Structure Folding 34
Fluorescence 36
Discussion 39
Chapter 3: Bulk Viscoelasticity of DNA 41
Introduction 41
Background: 41
Rheometers and Rheological Testing: 41
Viscoelasticity of DNA 44
Methods 45
Rheological Measurements 45
Results 46
Discussion 52
Chapter 4: Microrheology of DNA 54
Background 54

The Mathematics Behind Particle Diffusion 54
Particle Tracking 57
Methods 58
Sample Preparation 58
Microscopy and Image Processing 58
Results 59
Discussion 61
Conclusions and Future Work 63
Bibliography 65

List of Tables and Figures

Figure 1: The struture of double stranded DNA. Adapted from [1]. 10
Figure 2: A schematic of an immobilized Holliday junction, adopted from [4] . Half-arrows indicate the 5' end of the DNA strand. 12
Figure 3: The design of a DNA origami plate. Top: The design of a single staple complementary to three separate regions of the scaffold. Bottom: Scaffold routing, staple crossovers, and complementary staple design. 13
Figure 4: Collage of DNA origami structures. (a): Patterns on a DNA lattice, (b): Protein binding on an origami plate, (c): polymerization of DNA origami plates (d): Patterning of different macromolecules to make an origami face. Modified from [9]. 14
Figure 5: Schematic of material properties in shear and tensile modes. Dotted line indicates original shape, solid line indicates shape of material after deformation Δx and Δh due to force F applied over area A... 17
Figure 6: Comparison of stress and strain rate in Newtonian and non-Newtonian fluids. Viscosity is the ratio between stress and strain rate, the slope of the lines shown here. Newtonian fluids have a constant viscosity, while shear-thinning fluids have a viscosity that declines as a power law. 18
Figure 7: Comparison of different theoretical materials when subject to oscillating strain. The stress in the elastic material is perfectly in phase with the strain, while the viscous material is perfectly out of phase. The viscoelastic material is somewhere in between (here the phase lag is π/3). 20
Figure 8: Simplifying representation of a polymer of a series of beads and springs adapted from [20]. .. 21
Figure 9: Schematic of a polymer acting as an entropic spring. ΔS is the change in configuration entropy of the polymer due to deformation or relaxation. 22
Figure 10: Large particles (Red) surrounded by solvent (grey). B: The excluded volume represents volume inaccessible by solvent. Aggregation of large particles reduces exclusion volume. Modified from [22]... 23
Figure 10: Schematic of the Nanodyn. For clarity, only two of the six linkers are shown. Top left: Detail of the fluorescent oligonucleotides used. Top right, bottom right: Demonstration of the ability to constrain the Nanodyn. Bottom left: Cross section of the Nanodyn showing where the linker strands are. Modified from [25]. 28
Figure 11: The fluorescent spectra of Cy3 (left, donor) and Cy5 (right, acceptor), the FRET pair used in the Nanodyn. The blue lines show the emission spectra of each molecule, while the red lines show the emission spectra. The overlap (green) between the donor emission and the acceptor excitation spectra allows FRET to occur. Typical FRET excitation (yellow) and detection (red) ranges are highlighted. Adapted from [30]. 30
Figure 12: Gel electrophoresis image showing successful folding of the Nanodyn. From left to right, the lanes are: 10 kilobase DNA ladder, 8064 scaffold, Stock Nanodyn, Newly folded Nanodyn, 10 kilobase ladder. Red box indicates similarity between new structures and previously validated structures. Excess staples are seen near the bottom of the image. 34
Figure 13: TEM Image of several negatively stained Nanodyn structures in the open configuration. 35
Figure 14: Bulk Fluorescence spectra for the donor and acceptor attached to the Nanodyn. The peak at 670 nm corresponds to the excitation of the donor. The red curve shows more acceptor excitation because more of the Nanodyn are closed. 36
Figure 16: Nanodyn FRET Efficiency as a function of PEG-8000 weight percent. 37
Figure 17: Plot of FRET Efficiency vs Viscosity for the Nanodyn in varying PEG weight percentages. Viscosity calculated from [33], [34]. 38

Figure 16: A representative schematic of a parallel plate rheometer. The oscillating motor typically controls the bottom plate, while the top plate senses force. The sample (green) is held between the two plates. Adapted from [42]. 42
Figure 17: Common rheometer geometries: parallel plates (A), cone and plate (B), couette (C). Adapted from [43]. 43
Figure 18: The results of changing DNA concentration on the stress-strain relationship of the solution. Newtonian fluids have a constant linear stress-strain relationship. A decrease in slope is indicative of shear thinning. Error bars represent one standard deviation based on three replicates. 47
Figure 19: Plot of G' and G'' of 13 kbp DNA strands measured in an oscillatory strain sweep on a shear rheometer. Solid symbols are for G', while open symbols are G''. The oscillatory frequency was fixed at 1 rad/s. 1 dyne/cm^2 is equivalent to 0.1 Pa*s. Modified from [44]. 48
Figure 20: Viscoelastic Moduli from strain sweep of -DNA at varying concentration. The data show a decrease in the storage and loss moduli as concentration is decreased. Noise in the measurement prevented data from lower concentrations being added. Error bars represent 1 standard deviation based on 3 replicates. 49
Figure 21: Average stress vs strain for triplicate strain sweeps of 3 mg/ml CT-DNA at 3 frequencies. Both 1 rad/sec and 10 rad/sec were very noisy, and no signal was detected at 100 rad/sec at low strain. 51
Figure 22: Comparison of viscoelastic moduli in CT-DNA at varying concentrations. The data is very noisy, and it appears as though the elastic and viscous moduli are constant over the range of strains studied here. 52
Figure 23: Left: Representative frame of a microscopy video used for particle tracking. Right: Trajectories aquired from MATLAB particle tracking script 59
Figure 24: The trajectory of ten tracked beads is shown. In the picture above, the particle was tracked over 50 seconds. The displacement shown corresponds to a diffusivity of 2.28 μm^2/sec. 60
Figure 25: The difference between accepted literature values and measured values for the viscosity of water and 10% glycerol 61

Chapter 1: Introduction – DNA and Viscoelasticity

Background

This thesis encompasses several aspects: polymer physics, DNA nanotechnology, rheology, particle diffusion, and molecular crowding. Background information relating to all of these topics will be introduced in the following section to give context for the thesis motivation. Each chapter will include further background, which is relevant to the experimental details of the chapter.

DNA Origami

Deoxyribonucleic acid (DNA) molecules are biopolymers consisting of nucleotide monomers. The nucleotides consist of three components: A phosphate group, a deoxygenated ribose sugar, and a nitrogenous base. The first two are identical for any DNA nucleotide, but the nitrogenous base can be any of four unique molecules: cytosine, guanine, adenine, or thymine. The nitrogenous base identifies the nucleotide, and nucleotides are represented by the initial of their nucleobase: A for adenine, T for thymine, G for guanine, and C for cytosine (Figure 1, right). Sequences of letters represent polynucleotides with that sequence of bases. DNA strands have a directionality typically noted as 5’ to 3’ where the five prime (5’) end has a terminal phosphate, and the three prime (3’) end has a terminal sugar.

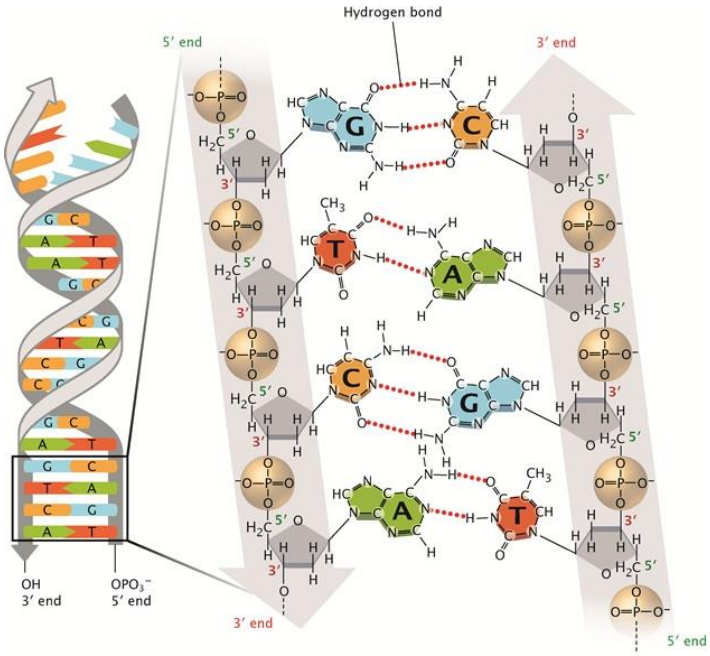

Figure 1: The structure of double stranded DNA. Adapted from [1].

If two DNA molecules are complementary, they can form a double helix (Figure 1) [2]. Complementarity of DNA molecules is governed by their sequence of bases. Adenine and thymine are complementary, as are cytosine and guanine. This complementarity is due primarily to two factors, hydrogen bonding and molecular size. Adenine and Guanine are purines, larger molecules containing two aromatic rings. Cytosine and thymine are pyrimidines, which are smaller and only have one aromatic ring. Due to the size of the double helix, a purine can only be complementary with a pyrimidine. Furthermore, A and T bind via two hydrogen bonds, while C and G bind via three. This combination of size and energetic constraints enforces the complementarity of DNA base pairing (A-T, C-G) [2]. DNA duplexes bind in an antiparallel configuration, with one strand running 5’ to 3’ and the other strand running 3’ to 5’ (Fig. 1).

DNA double helix formation is a chemical reaction, with a corresponding change in free energy, enthalpy, and entropy. There is a loss of entropy when two single-stranded DNA molecules combine, which must be offset by binding interactions between the strands mediated in part by hydrogen

bonding between bases. They are also stabilized by base stacking – the interaction of pi orbital electrons in successive bases [3]. The double helix constrains the geometry of the DNA, enabling base stacking interactions. Repulsion between the negatively charged phosphate backbones of DNA duplexes also creates an energetic cost for the formation of a DNA duplex. Thus, DNA duplexes must form in solution with positive ions, which screen the repulsions the negative phosphate group and stabilizes the double helix. This is particularly important for DNA assemblies like DNA origami where many helices are being packed tightly together. For DNA strands to self-assemble, the favorable energetic interactions from forming a DNA duplex must off-set the unfavorable loss of entropy and electrostatics. Since the effect of entropy is temperature-dependent, DNA duplexes will melt at a high enough temperature. The melting temperature occurs at the point where entropic effects overcome the stabilizing interactions of the duplex, causing it to fall apart. It is also worth noting that DNA duplexes do not require perfect complementarity between strands to form. As long as the stabilizing interactions between strands are greater than the loss of entropy at a given temperature, the duplex can form. It is also possible for a DNA strand to bind to itself, forming a hairpin loop, if two portions of the same single-stranded DNA are complementary. These variations on DNA secondary structures become important considerations in the design of DNA nanostructures, and in some cases they can be exploited to enhance the function of DNA nanodevices.

The first use of DNA as a nanoscale structural material was published by Nadrian Seeman in 1982 [4]. He used immobilized Holliday junctions to create repeating lattices of DNA. A Holliday junction

is a naturally occurring DNA structure which integrates four single-stranded DNA molecules (Figure 2).

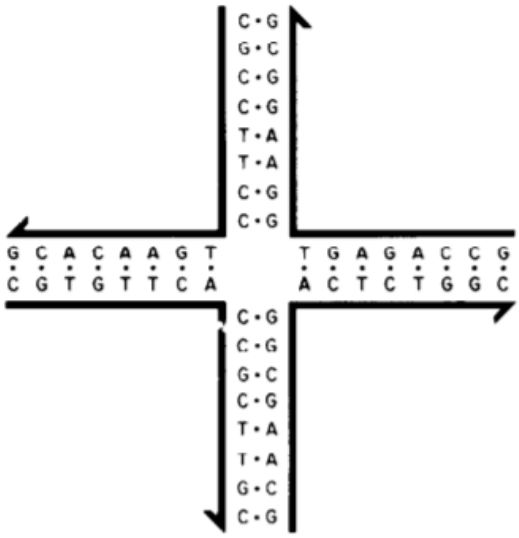

Figure 2: A schematic of an immobilized Holliday junction, adopted from [4] . Half-arrows indicate the 5' end of the DNA strand.

As shown in Figure 2, each DNA strand forms a double helix with two of the other strands. DNA molecules can be designed to create 2-D and 3-D DNA structures incorporating repeating Holliday junction motifs.

DNA origami nanostructures usually consist of several helices created by the base pairing of complementary DNA to form a series of stacked Holliday junctions. The technique was first introduced by Paul Rothemund in 2006 [5]. One loop of DNA, the scaffold, runs continuously through the whole structure. The scaffold, typically derived from the M13mp18 bacteriophage genome, has a length of 7000-8000 bases [6]. The wild type genome is 7249 bases with a fully known sequence. The length of the scaffold can be modified with specific DNA inserts which also have a known sequence. Based on the desired shape and the sequence of the scaffold, individual oligonucleotides known as staples can be synthesized which are complementary to specific parts of the scaffold. The staples bind to the scaffold in a piecewise complementary manner, pulling it into the desired shape (Figure 3, a DNA origami plate).

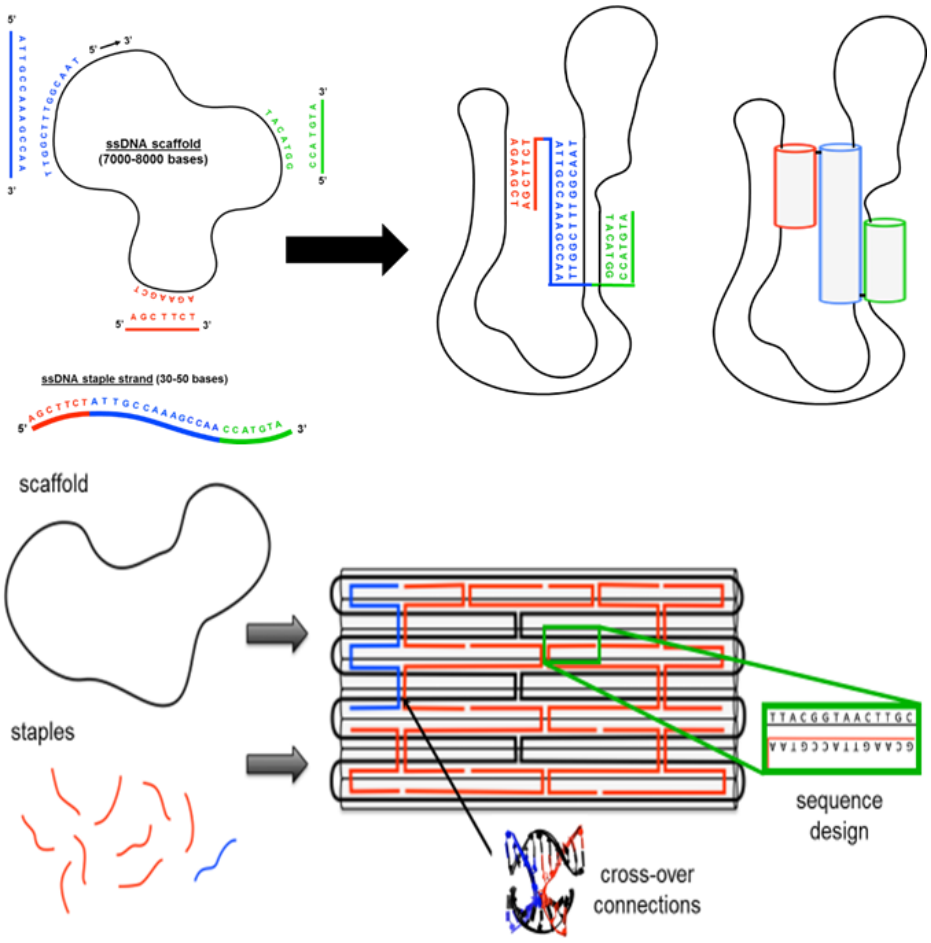

Figure 3: The design of a DNA origami plate. Top: The design of a single staple complementary to three separate regions of the scaffold. Bottom: Scaffold routing, staple crossovers, and complementary staple design.

The staples are designed such that they will cross over between adjacent double helices, stabilizing the structure. The placement and number of these cross overs is one contributor of structure viability – if there are not enough, the adjacent double helices will not be held together and the structure will not form.

To make DNA nanostructures, the scaffold and staples are first combined in a buffered salt solution [7]. The salt, typically $MgCl_2$, contributes cations to solution, which are necessary to stabilize the formation of double helices. DNA origami is folded in a thermal ramp, where it is typically heated to 65°C and cooled over a time period that can vary from hours to a few days. Initially, the high temperature of the thermal ramp melts DNA binding interactions including secondary structure of the

scaffold or staples. Secondary structure refers to instances in the scaffold or staples where there is self-complementarity and the DNA forms loops. Secondary structure in the scaffold or staples make it very unlikely that scaffold-staple binding will occur, and hence inhibits the formation of the desired nanostructure. The cooling step allows the staples to anneal to the desired region of the scaffold. The annealing of different staples takes place at different temperatures, partially governed by the base sequence of the double helix. Staple annealing is also cooperative; as staples bind with the scaffold, they constrain the scaffold loop and making it easier for other staples to bind [8].

DNA origami has developed substantially since it was first introduced in 2006. Rothemund initially demonstrated the flexibility of DNA origami by designing and synthesizing a number of two dimensional DNA origami structures including a rectangles, smiley faces, and triangles composed of adjacent DNA helices [5]. Further developments led to greater control over static DNA shapes, and the synthesis of three-dimensional shapes [6].

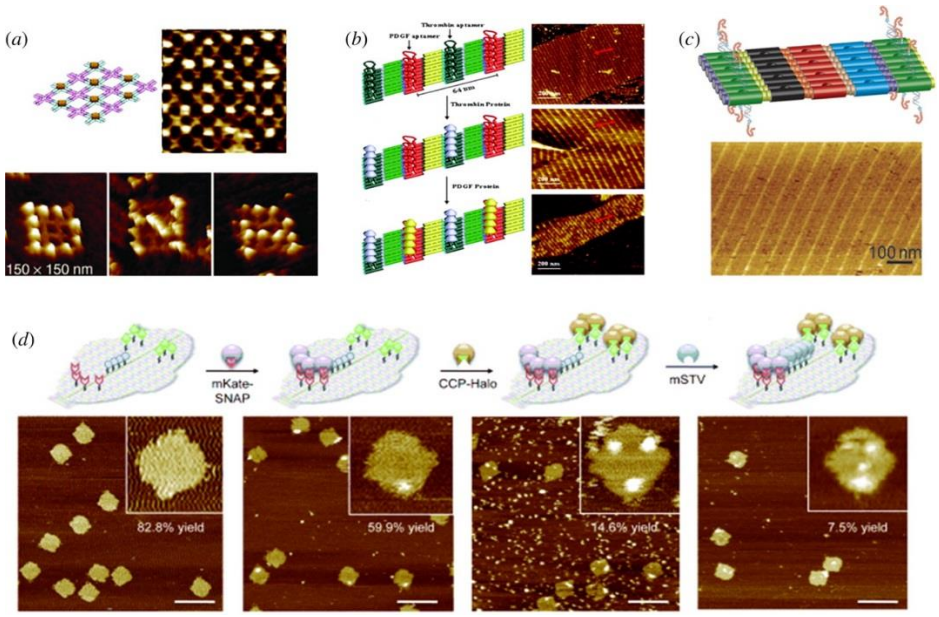

Figure 4: Collage of DNA origami structures. (a): Patterns on a DNA lattice, (b): Protein binding on an origami plate, (c): polymerization of DNA origami plates (d): Patterning of different macromolecules to make an origami face. Modified from [9].

In ten years, the scope of DNA origami has expanded dramatically (figure 4). DNA robots have been developed, which can undergo actuated conformational changes or walk along a pathway [10], [11]. DNA origami structures have been built which incorporate fluorophores or nanoparticles which can serve as sensors [12]. Several promising drug delivery devices have been produced which incorporate targeting and controlled release [13], [14]. These devices have shown great promise in *in vivo* mouse trials.

The simplicity of the DNA origami folding process belies the complexity of the reactions occurring to create the nanostructures. For every binding interaction between a portion of the scaffold and a portion of a staple, there is a thermodynamic equilibrium between bound and unbound DNA governed by the DNA base sequence. The temperature at which binding will occur is determined by the base sequence in addition to other factors such as scaffold looping entropy and cooperative binding effects. In addition to thermodynamic considerations, so called “Kinetic traps” can arise trapping the DNA origami structure in misfolded states that are local energy minima [7]. Kinetic traps were relatively easy to avoid for early 2D DNA origami structures, because the scaffold generally adopts a simple topology in the final structure. However, more complex shapes require more complex scaffold topologies giving rise to more complicated folding pathways and a higher probability of kinetic traps. Theoretical frameworks to understand DNA origami self-assembly and structure properties have necessarily advanced. The effect of staple arrangements on structure folding and cooperativity was explored by Wei et. al. and it was shown that energetically identical staples with different crossover locations change the overall thermodynamics of an origami structure [8]. Song et. al. demonstrated isothermal origami assembly at viable yield by changing the chemical composition of the solution [15]. Finally, Marras et al. showed that deliberate manipulation of the folding pathway of an origami structure can enable the creation of complex structures that are otherwise energetically unfavorable [16]. However, no one has studied the bulk physical properties of solutions containing DNA origami staples,

scaffold, or folded structures. DNA origami nanostructures are essentially rigid, while DNA molecules act as flexible chains in solution [17], [18]. The transition is gradual – different double-helical domains form as individual staples bind, gradually constraining the scaffold until it forms a well-folded, rigid structure. Studying this transition may provide new insights into how DNA origami structures form.

Rheology

Rheology is the study of the flow of matter. This can mean anything from the high temperature material creep of steel beams to the flow of water, but rheological measurements are most often used to study complex materials like colloid suspensions, solid and liquid polymers, and biological materials. A macro scale deformation of a material is generally a result of changes in the underlying structure down to the molecular scale, meaning that rheological measurements are fundamentally linked to the molecular character of the material. For polymers in solution, imposing a force on the bulk solution causes individual polymers to deform and changes in intermolecular interactions mediated by entanglements, cross-links or hydrodynamics. As a polymer, DNA can undergo similar deformation or interactions with the environment, and hence can be characterized by rheology.

Rheological measurements typically involve the application of a force and the measurement of the resulting deformation, or the measurement of a force required to achieve a specific deformation. For instance, a rubber sample will be stretched to double its length, and the required force will be measured. A critical feature of rheological measurements is the time scale and directionality of the imposed force or deformation and corresponding material response. As an example, stretching a sample of silly putty or bread dough by some amount over the time scale of a day might require less force than stretching that sample the same amount over the timescale of a second. This is an example of a viscoelastic material. In some cases, the direction of the test is also important. For example, deformation under an applied tension may be governed by a different material property than twisting

under a shear force or contraction under compressive force. This is an example of an anisotropic material.

Applied forces are typically expressed as stress, the force per unit area, and deformation is typically expressed as dimensionless strain. Rheological measurements typically quantify a relation between force and deformation, often characterized as a modulus – the ratio of stress to strain.

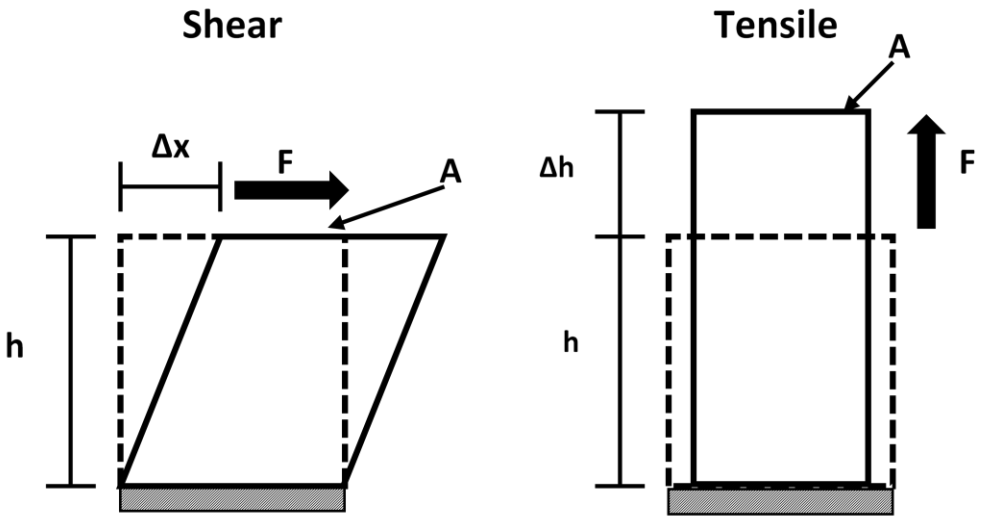

Figure 5: Schematic of material properties in shear and tensile modes. Dotted line indicates original shape, solid line indicates shape of material after deformation Δx and Δh due to force F applied over area A

A familiar example of a modulus is the elastic spring constant, where the modulus is the ratio of force to spring deformation. A stiff spring has a higher modulus. A schematic showing stress and strain in tensile and shear modes is given in figure 5. Based on figure 5, the equations relating stress (equation 1), strain (equation 2), and modulus (equation 3) in shear and tensile tests are:

	Shear	Tensile	
Stress:	$\tau = \frac{F}{A}$	$\sigma = \frac{F}{A}$	(1)

Strain: $\gamma = \frac{\Delta x}{h}$ $\epsilon = \frac{\Delta h}{h}$ (2)

Modulus: $G = \frac{\tau}{\gamma}$ $E = \frac{\sigma}{\epsilon}$ (3)

Strain, being a ratio of displacements, is dimensionless. Stress and modulus both have units of pressure.

Characterization of stress versus strain relations are some of the most fundamental rheological measurements, but they are not sufficient for the study of polymer solutions. Another important measurement is viscosity, the resistance of a fluid to flow. Whereas the modulus of a material is the ratio of stress to strain, viscosity is the ratio of shear stress to shear strain rate (Equation 4).

$$\eta = \frac{\tau}{\dot{\gamma}} \quad (4)$$

In a highly viscous fluid, more stress will be required to cause the fluid to flow at a given rate than in a low viscosity fluid. Viscosity can also be a function of shear rate, as is demonstrated in figure 6, below.

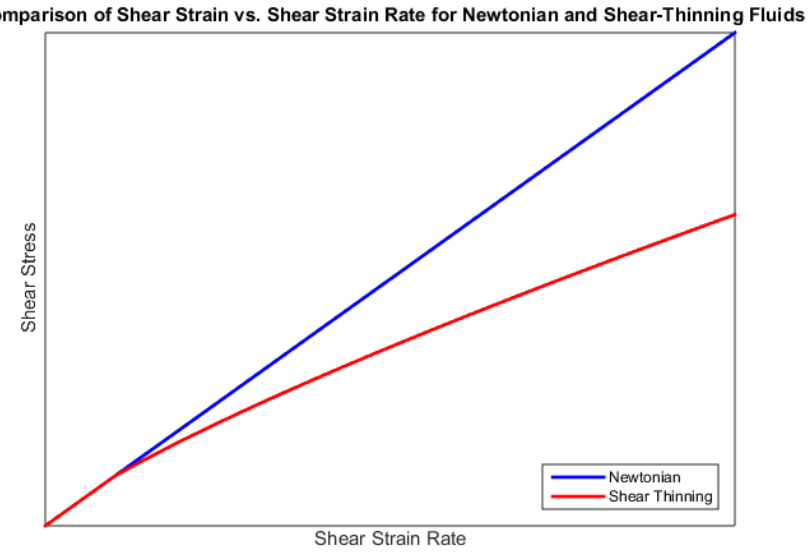

Figure 6: Comparison of stress and strain rate in Newtonian and non-Newtonian fluids. Viscosity is the ratio between stress and strain rate, the slope of the lines shown here. Newtonian fluids have a constant viscosity, while shear-thinning fluids have a viscosity that declines as a power law.

The viscosity of Newtonian fluids is independent of strain rate – twice as much shear stress will double the shear strain rate. However, this relationship does not hold for a shear thinning fluid, which is typical

of a high concentration polymer solution. At low shear rates, the viscosity of a concentrated polymer solution is relatively high. This is due to the entanglement of polymer molecules and the greater degree of interaction between polymers in an equilibrium configuration. However, as shear is continuously applied, the entanglements of molecules are broken and the individual molecules are deformed into a straighter configuration, where polymer molecules can slide past each other relatively easily. This leads to a decrease in viscosity. Similar molecular deformations can lead to strain hardening in polymeric solids since polymers become harder to stretch once they are closed to their extended configuration or can undergo strain induced crystallization once molecules are aligned under deformation.

Some materials can be described by adequately by either their modulus – as in a steel beam, or their viscosity – as with a Newtonian fluid like water. However, most materials have viscous and elastic qualities. They are viscoelastic. Rheology is primarily concerned with the measure of viscoelasticity in solid and liquid samples. Viscoelasticity is typically measured using oscillatory stress or strain. In an oscillatory strain test, the applied shear strain (equation 5) and shear strain rate (equation 6) are described by the following equations:

$$\gamma = \gamma_0 \sin(\omega t) \tag{5}$$

$$\dot{\gamma} = \gamma_0 \omega \cos(\omega t) \tag{6}$$

where ω is the frequency of oscillation and γ_0 is the maximum strain magnitude. The resulting stress in a viscoelastic material is then given by:

$$\tau = \tau_0 \sin(\omega t + \delta) \tag{7}$$

where δ is the phase lag. For a perfectly elastic material, the phase lag will be zero – the stress will be exactly in phase with the applied strain. For an entirely viscous material, stress is related to the derivative of the strain, so the phase lag will be 90°. A viscoelastic material will have a phase lag

between 0° and 90°, corresponding to the relative energy dissipation and storage. Each of these behaviors is shown in Figure 7.

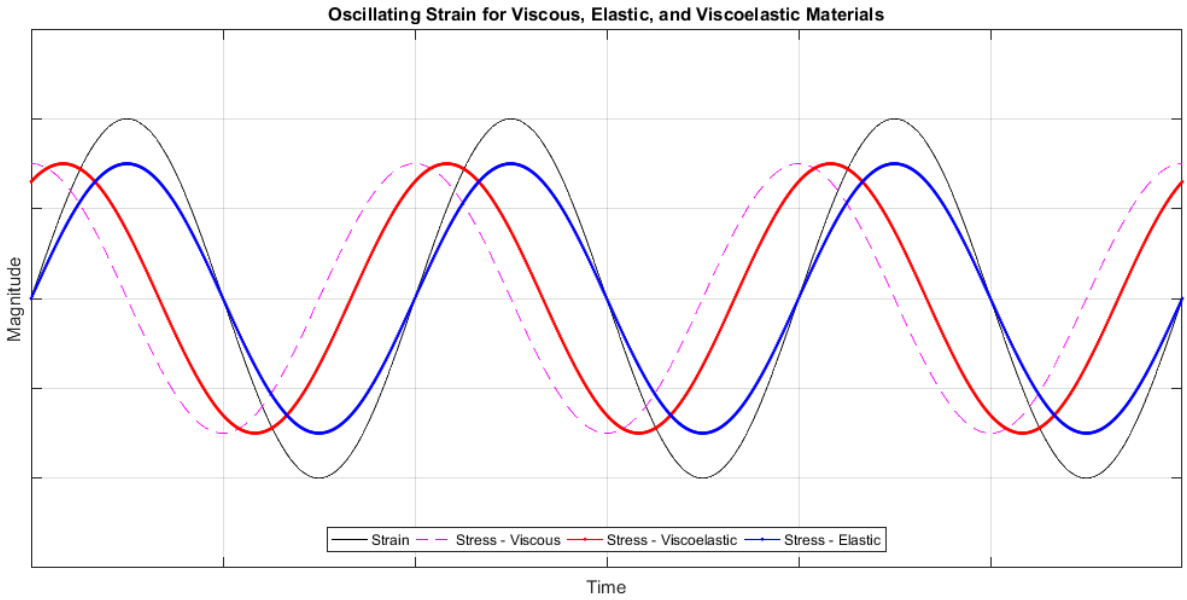

Figure 7: Comparison of different theoretical materials when subject to oscillating strain. The stress in the elastic material is perfectly in phase with the strain, while the viscous material is perfectly out of phase. The viscoelastic material is somewhere in between (here the phase lag is π/3).

From the phase lag, storage modulus G' and loss modulus G'' are defined in equations 8 and 9, below. The storage modulus is the component of the modulus which is in phase with the strain, while the loss modulus is the component that is 90° out of phase with the strain.

$$G' = \frac{\tau_0}{\gamma_0}\cos(\delta) \tag{8}$$

$$G'' = \frac{\tau_0}{\gamma_0}\sin(\delta) \tag{9}$$

The same conventions for shear and tensile modes hold; when referring to moduli, G denotes shear while E denotes tensile modulus.

There are several models that account for the viscoelasticity of polymer solutions. One of the simplest, the rouse model, treats polymers as a series of beads and springs (figure 8) [19]. The springs model the polymer elasticity, while the beads experience viscous hydrodynamic drag.

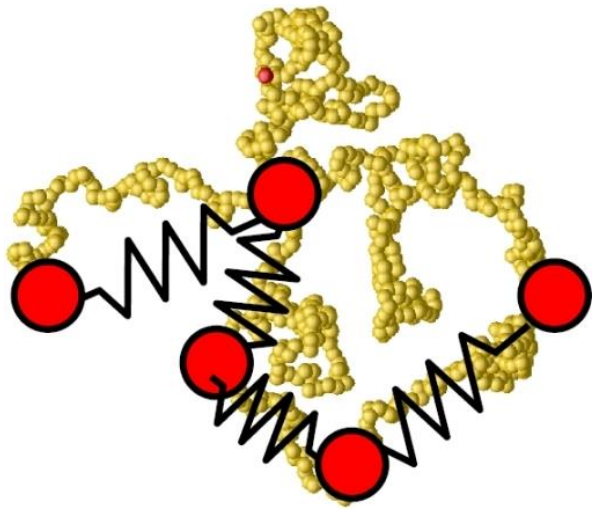

Figure 8: Simplifying representation of a polymer of a series of beads and springs adapted from [20].

For the Rouse model the polymer chain is broken down into segments where each segment behaves as an elastic spring. The rouse model is only applicable when the length of the chain is much greater than the length of each subunit. The beads capture the energy is dissipated from the hydrodynamic drag the chain experiences as it moves through the solution, while the springs capture the energy stored via the entropic elasticity of the polymer. The rouse model can be used to understand how a macromolecule behaves in a solution subject to flow. The beads are subject to hydrodynamic drag forces, causing the molecule to align with the flow and stretching the springs connecting the beads. The stretched springs store energy. When flow stops, the stretched springs relax, causing the beads to move. The beads once again experience drag forces, dissipating some of the energy stored.

In solution, polymer molecules have an equilibrium distribution of conformations. The most likely conformation at equilibrium represents the minimum free energy for the chain, which is a function of the configurational entropy of the chain, interactions between the polymer and the solvent, and any potential inter- or intra-molecular interactions. Ignoring intra- or inter-molecular interactions, when the polymer is deformed, the configurational entropy is decreased.

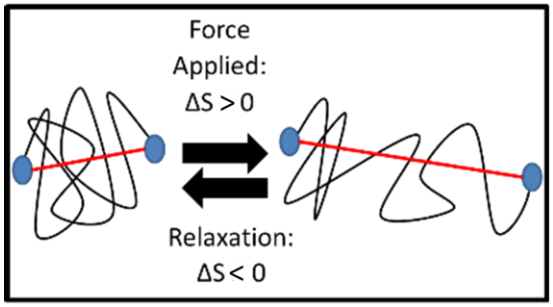

Figure 9: Schematic of a polymer acting as an entropic spring. ΔS is the change in configuration entropy of the polymer due to deformation or relaxation.

Therefore, increasing entropy acts as a restoring force for the molecule. This process is shown for an individual macromolecule in figure 9.

The Rouse model was conceived to describe the behavior of dilute polymers in solution. In this case, *dilute* has a very specific meaning: separate polymer chains do not interact. Significant interactions between polymers lead to longer timescale behaviors that the Rouse model cannot account for. The overlap concentration, c*, which is the concentration where polymer molecules start to overlap can be approximated by the formula:

$$c^* = \frac{\rho N}{R_g^3} \tag{10}$$

where ρ is the mass density of the chain, N is the number of monomer units in the chain, and R_g is the radius of gyration for the molecule [21]. The radius of gyration is a measure of the average distance from the polymer center of mass to a monomer unit.

Molecular Crowding:

The presence of macromolecules in solution can cause polymers to store or dissipate energy differently, affecting their rheology. However, macromolecules in solution are also responsible for another effect: molecular crowding. Molecular crowding leads to depletion forces that tend to be compressive forces on a molecule or structure. Depletion forces arise in solutions of macromolecular

solutes surrounded by relatively smaller molecules that are on the same size scale (Figure 10). These molecules are typically represented as hard spheres with dimensions given by the interaction distance of the molecule.

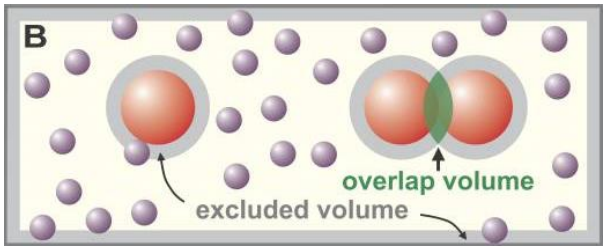

Figure 10: Large particles (Red) surrounded by solvent (grey). B: The excluded volume represents volume inaccessible by solvent. Aggregation of large particles reduces exclusion volume. Modified from [22].

Depletion forces are typically understood as totally entropic. As shown in figure 10, there is some excluded volume surrounding each macromolecule, and at the border of the box. The excluded volume is space that is inaccessible to crowding molecules due to their size. The maximum entropy of the full system is related to the volume accessible by the crowding molecules. Minimizing the excluded volume leads to higher entropy of the crowding molecules. The excluded volume in the system is a function of the size of the crowding molecule and the size of the macromolecule. Assuming neither changes size, the excluded volume due to an individual macromolecule cannot be changed. However, when macromolecules aggregate their excluded volume overlaps (Figure 10), decreasing the total excluded volume in the system. Reducing the excluded volume also reduces the entropy, giving rise to a depletion forces pushing the macromolecules together that is a function of the crowding molecule concentration.

Cells are full of macromolecules of different compositions, so it is unsurprising that depletion forces are significant in many cellular functions. It has been shown that molecular crowding forces are comparable to the forces involved in many cellular activities. For instance, the formation of higher order structures in proteins and DNA, and it has been shown that molecular crowding increases the rate of

refolding of various enzymes [22]. Crowding molecules increase the melting temperature of DNA duplexes and affect organization of DNA at the chromatin level [23]. There are several other examples of molecular crowding contributing to biochemical phenomena in literature.

Significance:

DNA origami clearly has potential to address many critical challenges in medicine and nanoscience, including drug delivery, diagnosis, and molecular detection. More visionary applications of DNA origami include information storage and computing. A better understanding of the self-assembly process to maximize yield, efficiency, repeatability, and scalability is essential for DNA origami to leave the lab and fulfill its industrial and clinical potential.

DNA origami folding is complex. Dozens of polymer molecules bind non-covalently. The configuration of the polymers must change to accommodate these new bonds. Due to the energy involved in staple binding and the topology of the molecules, subtle changes in staple arrangement can yield very different results. The analysis of DNA binding is further complicated by the chemical nature of the bonds formed. Double helices are stabilized by hydrogen bonding between adjacent bases, and all of the hydrogen bonds are essentially identical. Given the similarity of bonds formed, typical spectroscopic methods are useless for differentiating between them. By conjugating a fluorophore to a specific staple, the binding of that staple can be studied, but this approach does not scale well given that more than one hundred staples are involved with origami folding. The chemical binding of two different staples is almost identical, but their effect on the scaffold can be very different. One staple might pull three separate regions of the scaffold together in space, while another one might bind to one continuous region of the scaffold, having very little effect on the scaffold shape. Therefore, exploring the physical effect of staple binding may provide new insight into understanding and optimizing DNA origami folding.

Molecular crowding and rheology are intimately connected. The hierarchal folding of proteins bears some resemblance to the cooperative folding of DNA origami. Therefore, determining if crowding could be used to influence origami folding could improve the yield of origami folding or allow for the formation of new structures. For instance, the binding of DNA origami staples is concentration dependent, and putting more of a particular staple in solution will increase the rate at which that particular staple binds. However, staples may also act as crowding agents, and crowding may affect the conformation of the scaffold, inhibiting folding. Improving the understanding of DNA viscoelasticity and its relationship with molecular crowding could also be beneficial for enhancing DNA origami production.

Furthermore, because folded DNA origami structures are affected by molecular crowding it should be possible to study the effects of molecular crowding, and consequently rheology, using DNA origami nanostructures. DNA origami is inherently biocompatible and other applications of DNA origami have demonstrated that it is stable in cell cytosol for hours [24]. DNA origami could be used to measure the effects of molecular crowding and rheology in cells, which would provide valuable new understanding related to how cellular viscoelasticity affects cellular processes.

Objective:

This thesis will work towards connecting rheology and molecular crowding with DNA origami. The long-term goal of this work is to test how the rheology of a DNA origami solution changes as it forms compact nanostructures from disparate strands of DNA. I hypothesize that, as the scaffold and staple molecules become more constrained, their behavior will change. Specifically, the conformations of the DNA stands in solution is changing, which should affect their interactions both with the solvent and other molecules, and the number of bulk staples in solution decreases, likely leading to less energy dissipation.

Along with studying the evolution of rheological properties during folding, the effect of physical interactions with surrounding solvent on folded DNA origami nanostructures was studied. A two state (open/closed) nanostructure called the Nanodyn had been developed previously [25]. It has been demonstrated that the Nanodyn conformation is sensitive to changes in viscosity. The sensor shows potential for studying viscoelasticity and molecular crowding, but it needs to be fully characterized. Therefore, the variation in sensor output was measured over a range of viscosities. Viscosity was controlled by changing the amount of polyethylene glycol in solution. This work will contribute to the use of the sensor for measuring the viscoelastic properties of collagen matrices. Collagen is a structural protein which is common in the extracellular matrix. It has been shown that reorganization of collagen and stiffening of tissue is a characteristic of tumors, but it is difficult to measure that stiffening locally [26]. Measuring the behavior of the Nanodyn implanted in collagen may improve our understanding of the role of tissue stiffening in cancer.

Chapter 2: Molecular Crowding and DNA Origami

Introduction

Dynamic DNA origami devices typically have a distribution of configurations defined by the energy landscape of the structure [27]. Given the comparable size of DNA origami and biomolecules, it is likely that the conformation DNA origami could be affected by molecular crowding. Therefore, the use of DNA origami for studying molecular crowding was explored.

Background

The design and functionality of the DNA origami device will be detailed in the following section, and background will be given for the analysis methods used for the device.

The Nanodyn:

The NanoDyn, a DNA origami device developed at Ohio State by Dr. Michael Hudoba, was used to test the hypothesis that DNA origami nanostructures are affected by molecular crowding [25]. The NanoDyn is a two state (open/closed) nanostructure that incorporates fluorescent molecules to indicate the state of the device. Each barrel of the Nanodyn has a 24 helix bundle cross-section, and the barrels are approximately 50 nm long (Figure 11). The barrels are connected by six scaffold loops arranged radially around the barrels. Each scaffold loop is relatively unconstrained, allowing the barrel to switch between the open state, where the barrels are far apart, and the closed state, where they are close together.

The addition of constraining staples can specifically modify the dynamics of the device. Typically, staples are added that are complementary to the scaffold loop, turning into two dsDNA duplex sections connected end-to-end but separated by a few ssDNA bases to facilitate flexible motion between the two barrel components. Alternatively, constraining staples can be added to pull individual scaffold loop

together, forcing the device to close and biasing the conformation of the device overwhelmingly towards the closed state. Further details relating to the Nanodyn can be found in reference [25].

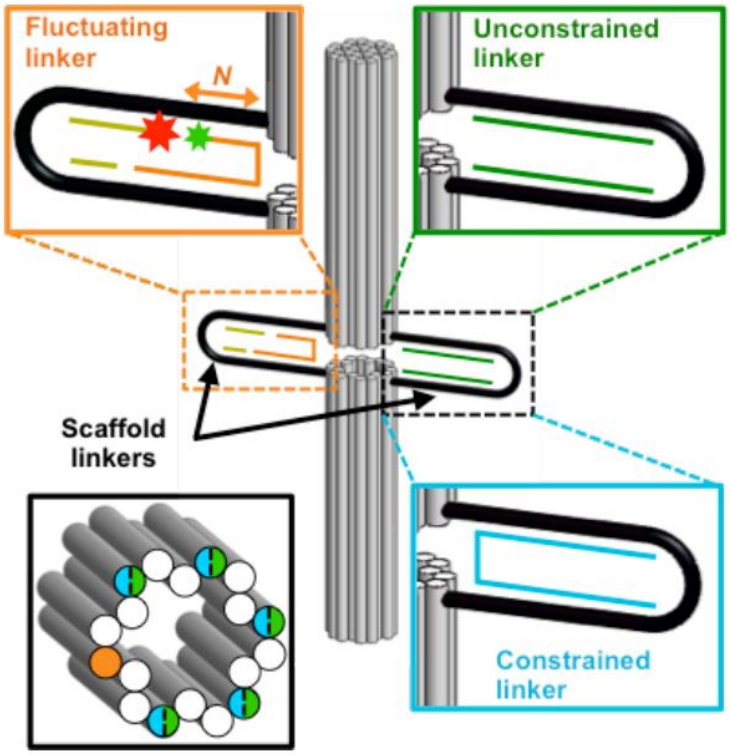

Figure 11: Schematic of the Nanodyn. For clarity, only two of the six linkers are shown. Top left: Detail of the fluorescent oligonucleotides used. Top right, bottom right: Demonstration of the ability to constrain the Nanodyn. Bottom left: Cross section of the Nanodyn showing where the linker strands are. Modified from [25].

The loops can also be constrained using fluctuating staples – these staples are designed to bind with a high affinity to one portion of the scaffold loop, while binding transiently with another portion (figure 11, top left). The fluctuating linkers impart dynamic opening and closing behavior where the dwell times in the closed state can easily be tuned by the strength of the transient binding interaction. For example, a fluctuating linker binding between eight nucleotides will close for a very short time that might not even be detectible with typical measurement methods. Alternatively considering many Nanodyn devices at a single point in time, only a very small fraction would be closed. In contrast, a longer connection of

twelve bases would lead to longer dwell times in the closed state, or close a much larger portion of the population at a single point in time. We assume the opening/closing is an ergodic process such that the behavior of a single device over long times can recapitulate similar behavior compared to considering many devices at a single point in time. In addition, up to five scaffold loops can be constrained individually (Fig. 11, bottom right), giving precise control over the dynamics of the device.

Förster Resonance Energy Transfer

By conjugating the fluctuating linker staples with fluorescent molecules, the dynamics of the device can be studied using fluorescence-based techniques. Two fluorescent molecules can interact when they are very close (<10 nm), in a phenomena known as Förster resonance energy transfer (FRET) [28], [29]. The interaction is a strong function of distance, meaning that FRET can be used to detect changes in distance at the nanoscale.

FRET is the non-radiative transfer of energy between two fluorescent molecules, a donor and an acceptor. Any fluorescent molecule has a characteristic absorption and emission spectra, which describes the range of wavelengths of light that can excite it and the range of wavelengths it will emit light at. FRET is a function of spectral overlap between the donor emission spectrum and acceptor excitation spectrum. The fluorescence spectra of Cy3 and Cy5 is shown in the following figure (Figure 12).

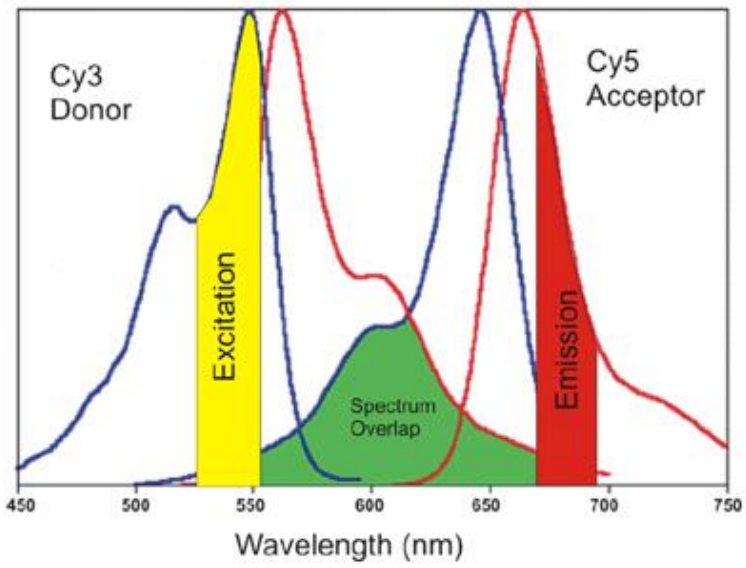

Figure 12: The fluorescent spectra of Cy3 (left, donor) and Cy5 (right, acceptor), the FRET pair used in the Nanodyn. The blue lines show the emission spectra of each molecule, while the red lines show the emission spectra. The overlap (green) between the donor emission and the acceptor excitation spectra allows FRET to occur. Typical FRET excitation (yellow) and detection (red) ranges are highlighted. Adapted from [30].

Due to the large spectral overlap between Cy3 and Cy5, they are commonly used as a FRET pair and were incorporated into the Nanodyn. FRET is typically expressed as a normalized efficiency representing the amount of energy transferred from the donor to the acceptor normalized by the total intensity emitted by the combination of donor and acceptor.

FRET interactions are mediated by several factors other than spectral overlap, with distance being the most significant. The FRET efficiency for a single FRET pair is given the following formula:

$$E_{FRET} = \frac{R_0^6}{R_0^6 + r^6} \tag{11}$$

Where r is the distance between the fluorophores and R_0 is a dye specific constant related to the quantum yield of the donor dye, the orientation of the molecules, and the degree of overlap of the spectra of the dyes. The sensitivity of FRET to distance is caused by the dependency on distance to the sixth power, causing FRET efficiency to drop to approximately zero very quickly as the donor and acceptor separate.

Binding of the fluctuating linker will force the Nanodyn into its closed conformation, and dissociation of the fluctuating linker allows the structure is open. The displacements between the open and closed state are on the scale of ~10 nm, making FRET an appropriate readout. In the Nanodyn, the fluctuating staple is conjugated with one fluorophore, while the other fluorophore is conjugated with a staple that binds permanently with the scaffold loop (Figure 11). Therefore FRET efficiency will be directly correlated to the proportion of Nanodyn structures in the closed conformation. The fluorescent functionality of the Nanodyn is beneficial for several reasons. The conformation of the device can be observed and measured using other methods such as transmission electron microscopy (TEM), but those methods are typically incompatible with biological samples. Fluorescence is commonly used in biological assays, meaning the Nanodyn could be easily integrated into many biological systems.

Methods

There were several requirements for testing the hypothesis that the Nanodyn is sensitive to molecular crowding. Viable structures needed to be folded, purified, and validated. The solution viscosity needed to be controlled in a way that was compatible with DNA origami. Finally, the fluorescent output of the structures needed to be measured.

Structure Folding and Validation

The Nanodyn is designed to be folded with an 8,064 base long scaffold, and the oligonucleotides used to fold the structure were designed previously. Several aspects of the Nanodyn folding process have also been optimized previously [25]. Based on this previous work, the Nanodyn was folded at 18 mM $MgCl_2$ concentration. A 65 hour thermal ramp from 65°C to 4°C was used to fold the structure. The structure was folded at 20 nM scaffold concentration with 10x excess staples in folding buffer (5 mM TRIS, 1 mM EDTA, 18 mM $MgCl_2$, 5 mM NaCl) according to a standard procedure found in literature [7].

After structures were folded, they needed to be validated. Agarose gel electrophoresis is a method that applies a charge across a gel containing DNA samples. The negative charge of DNA causes it to migrate towards a positive electrode, while the size of the DNA changes the rate of migration. DNA origami structures are much more compact than the scaffold, so structures typically migrate more quickly than the scaffold but can vary depending on the specific geometry of the origami structure. The gels used to validate DNA origami were 2% agarose, made with .5X Tris-Borate-EDTA buffer and 11 mM $MgCl_2$. The gel was run at 70 volts until the scaffold and staples had sufficient time to separate.

Structure validation was further accomplished using transmission electron microscopy (TEM) [7]. For imaging DNA origami, the structures are deposited on a copper mesh grid, and 2% uranyl formate is subsequently added to produce a negative stain. The heavy uranium nuclei deflect the electron beam, while it passes straight through the DNA origami samples to a detector. To prepare TEM grids, 4 µl of origami structures were deposited on a plasma cleaned grid. After four minutes, the sample was wicked off of the grid. Finally, 10 µl and 20 µl beads of UFO and were added to the grid and it was dried. The TEM images were obtained using an FEI Tecnai G2 Biotwin electron microscope with an electron velocity of 80 kV.

Once well-folded structures were confirmed by gel electrophoresis and TEM, they could be used for experiments. To avoid the reduced concentrations associated with gel purification, we used a different purification method. For experiments folded origami structures were purified using a standard procedure developed by Stahl et al., poly-ethylene glycol (PEG) purification [31]. PEG purification is commonly used in other applications to purify DNA, and was applied to DNA origami fairly recently. To PEG purify DNA origami, 15% wt/v PEG-8000 with 5 mM Tris, 1 mM ETDA, and 500 nM NaCl was mixed with an equal volume of the folded Nanodyn. At least 200 µl of folded structure were purified. The PEG-origami mixture was centrifuged for 25 minutes at 16,000 g and at room temperature. The supernatant was removed from the tube using a pipette, and the resulting DNA origami pellet was resuspended in

the desired buffer. For the Nanodyn, the resuspension buffer used was typically 1x folding buffer and 10 mM $MgCl_2$. The PEG purification procedure can be repeated an arbitrary number of times – most staples are removed after one round, and after two rounds staples are almost nonexistent. The concentration of the resulting PEG purified solution was measured using a nanodrop spectrophotometer [7].

Fluorescence Measurements

To quantify FRET efficiency in the Nanodyn, a HORIBA Fluoromax fluorometer was used to excite samples with specific wavelengths of light and to measure their fluorescent output at a range of wavelengths. The sample was excited at 510 nm and the fluorescent intensity was measured from 530 – 750 nm. This excitation wavelength will directly excite the donor, and if FRET is occurring the acceptor will also be excited. The sample was also excited at 610 nm to directly excite the acceptor and intensity was measured from 630 – 750 nm. The resulting spectra were processed using the ratio A method, described elsewhere [32]. Briefly, FRET efficiency is obtained from the ratio(A) method calculating the ratio of acceptor excitation from donor excitation to direct acceptor excitation. The method used here also uses a blank spectra and a spectra of the bulk fluorophores to obtain a more precise measurement.

PEG purified Nanodyn samples were analyzed in a 12 µl quartz cuvette using the fluorometer. The Nanodyn structures were present at approximately 20 nM as measured by the nanodrop. Exact concentration measurements are not strictly necessary for fluorescence, because the ratio of emissions is calculated. As long as the concentration is high enough to obtain clear spectra, the efficiency of samples at differing concentrations can be compared.

The viscosity of the Nanodyn samples was controlled by varying the weight percentage of PEG-8000 in solution. After two rounds of PEG purification, the Nanodyn was resuspended in 1x FOB at 10 mM $MgCl_2$. Aliquots of the resulting PEG purified samples were combined in a 1:1 volumetric ratio with solutions of PEG-8000, also at 1x FOB and 10 mM $MgCl_2$, in order to obtain Nanodyn structures in PEG at

a known weight percent. Literature correlations for PEG viscosity were used to approximate the viscosity of the resulting solution.

Results

Structure Folding

Following the described procedure for folding the Nanodyn, viable structures were created. The results of gel electrophoresis comparing the scaffold with the folded structure can be seen in figure 13, below.

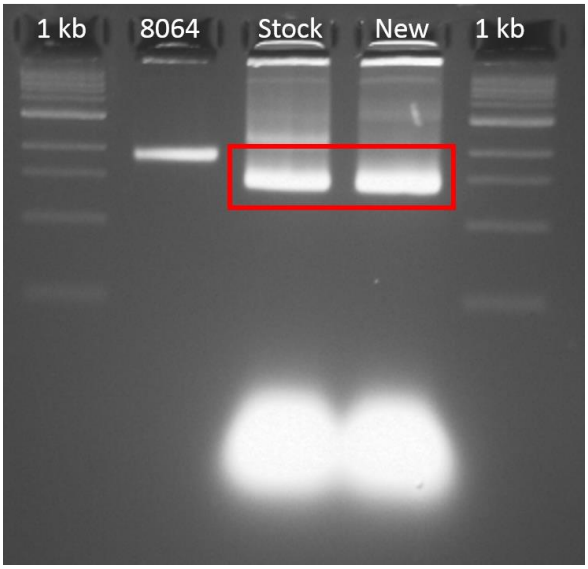

Figure 13: Gel electrophoresis image showing successful folding of the Nanodyn. From left to right, the lanes are: 10 kilobase DNA ladder, 8064 scaffold, Stock Nanodyn, Newly folded Nanodyn, 10 kilobase ladder. Red box indicates similarity between new structures and previously validated structures. Excess staples are seen near the bottom of the image.

The well-folded, compact structures travel faster than the scaffold, behavior which is consistent with most DNA origami structures. The “stock” Nanodyn is an identical nanostructure that was previously folded. It is used here to ensure that the newly folded structures match structures that have already been validated in previous work. The two are not identical – there is a secondary band in the stock that is not present in the new fold. This secondary band is probably a result or structure dimerization that sometimes occurs over time. Given sufficient time, interactions between structures can cause them to

dimerize or aggregate. Despite the secondary band in the stock well, the results of gel electrophoresis suggest that the newly folded Nanodyn closely resembles the previously validated structure.

To fully validate proper folding of the Nanodyn, the folded structures were PEG purified once. TEM grids were prepared with the structures and they were imaged. A representative image of the Nanodyn can be seen in figure 14.

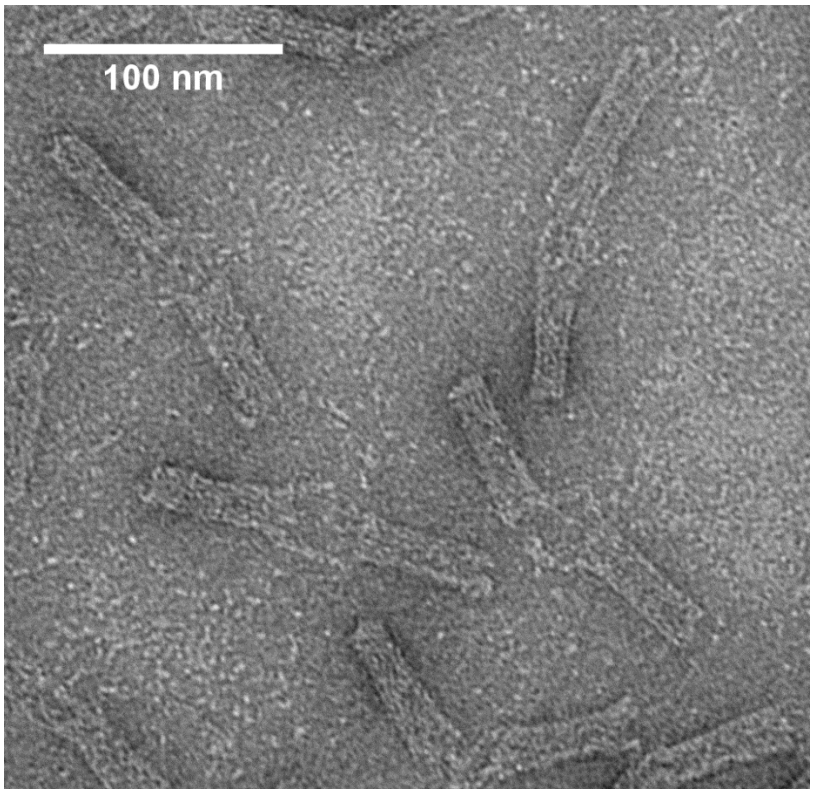

Figure 14: TEM Image of several negatively stained Nanodyn structures in the open configuration.

In figure 14, both barrels of the Nanodyn can clearly be seen, with a gap of approximately 35 nm between them in some places. This gap length is consistent with the length of the scaffold loops. The TEM images show that there is a distribution of configurations occupied by the Nanodyn. In figure 14, several Nanodyn are shown in a variety of open configurations.

Fluorescence

The validated structures at 20 nM were tested for bulk fluorescence across a range of PEG-8000 weight percentages. A constant salt and buffer concentration was maintained across samples to ensure the viability of the origami. The FRET efficiency was measured as described previously. The following image (figure 15) compares the normalized spectra of two samples, one in buffer (blue) and one in 15 wt% PEG-8000 (red). The intensities of each spectra were normalized to account for differences in concentration between samples.

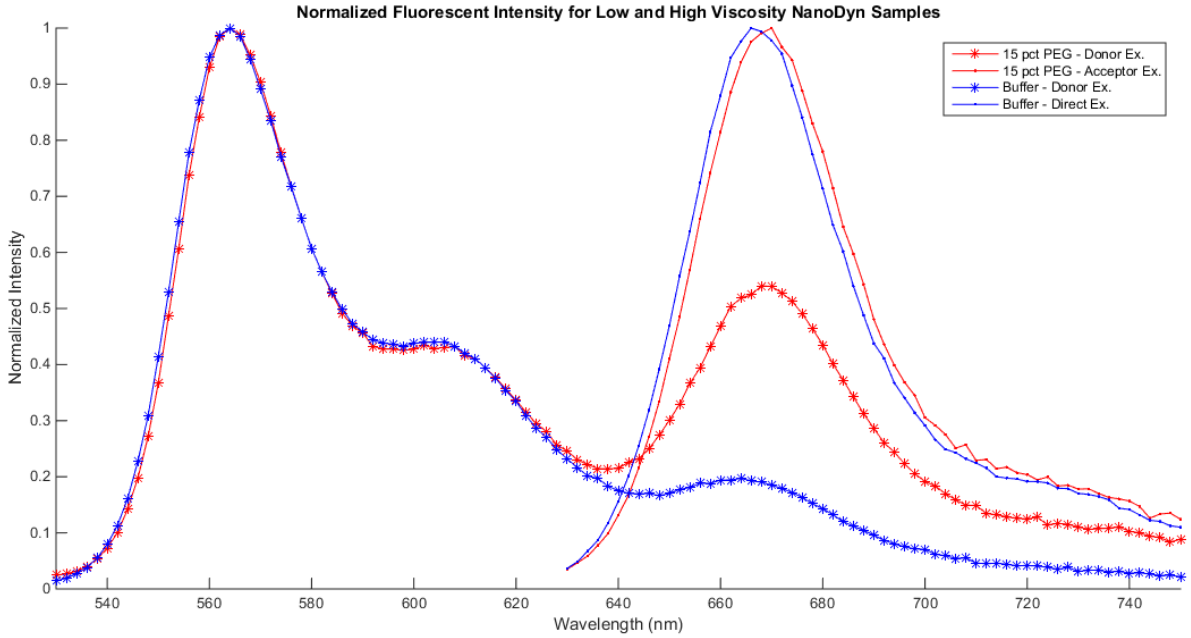

Figure 15: Bulk Fluorescence spectra for the donor and acceptor attached to the Nanodyn. The peak at 670 nm corresponds to the excitation of the donor. The red curve shows more acceptor excitation because more of the Nanodyn are closed.

The plots of direct acceptor excitation are almost identical, with a peak at 670 nm independent of PEG-8000 concentration. When the donor is excited, there is also an identical peak at 560 nm, independent of PEG concentration. However, the donor excitation spectra differ at 670 nm. There is a much higher peak at 670 nm due to the addition of PEG-8000 to the solution. This peak corresponds to the acceptor,

and indicates that more FRET is occurring from donor to acceptor in the PEG solution. This most probably indicates that more Nanodyn are closed in the more viscous solution.

Identical Nanodyn structures were diluted in a range of PEG-8000 concentrations, and the bulk fluorescence of each was measured. The FRET efficiency of each was calculated, and the results are shown in figure 16 and figure 17, below.

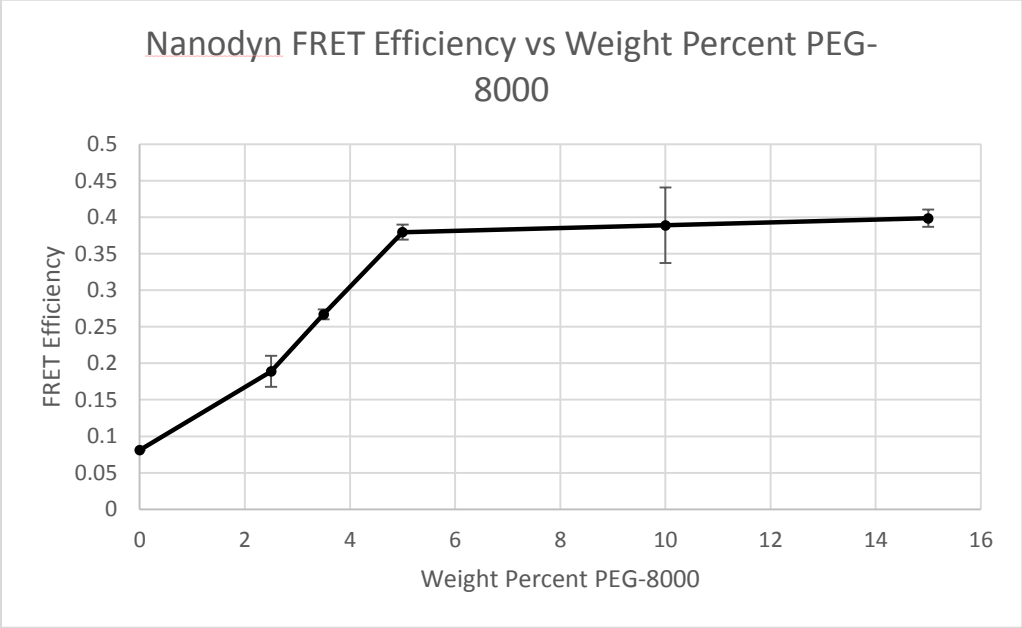

Figure 16: Nanodyn FRET Efficiency as a function of PEG-8000 weight percent.

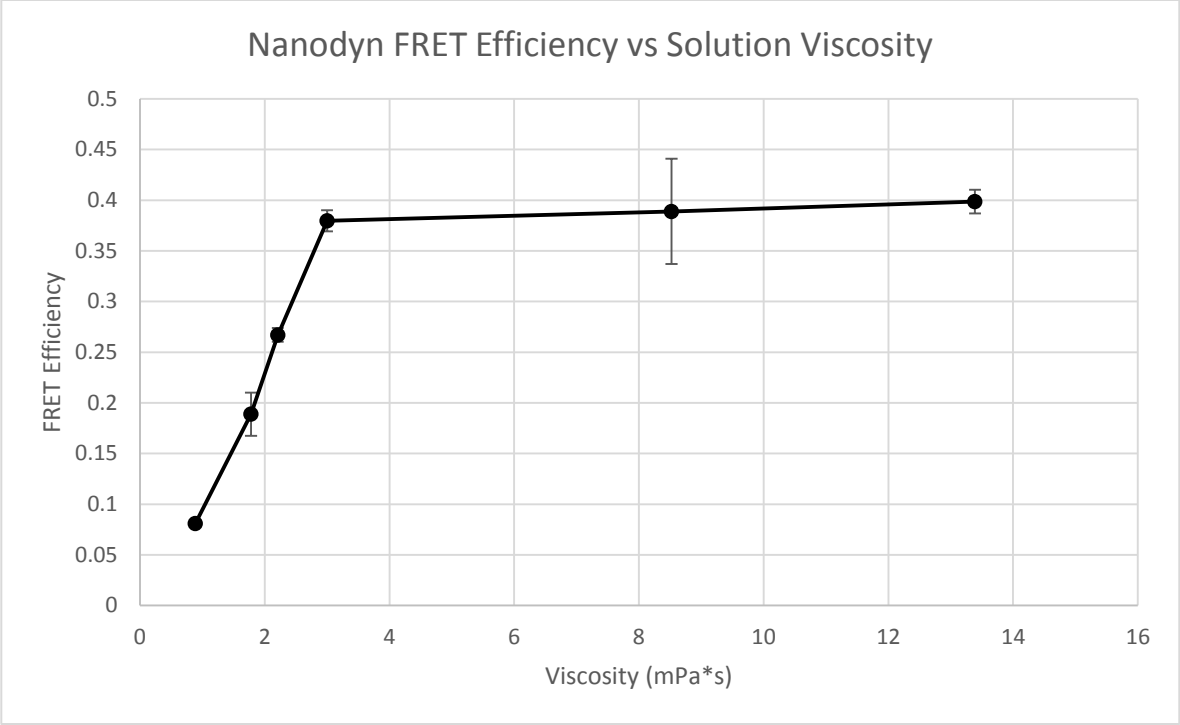

Figure 17: Plot of FRET Efficiency vs Viscosity for the Nanodyn in varying PEG weight percentages. Viscosity calculated from [33], [34].

The plot (figure 17) shows a clear linear dependence of FRET efficiency on viscosity in the lower range, before the efficiency settles to a relatively constant value around .38.

The dependence of viscosity on FRET efficiency indicates that the conformation of the Nanodyn is sensitive to the presence of macromolecules in solution. As the space available for the Nanodyn decreases, the entropic cost associated with the closed structure is decreased. This makes it more likely to exist in the closed state. It is unsurprising that this dependence is essentially linear at low viscosity, given that the Nanodyn mostly exists in an open state in buffer. However, the efficiency curve becomes saturated, as almost all of the Nanodyn exist in the closed conformation and no more can be closed. This corresponds with the plateau observed above 3 mPa*s. The efficiency does not reach 100% due to several possible reasons. As previously mentioned, FRET is a strong function of distance, and there is still some separation between fluorophores when the device is in the closed state. Further decreases in the

expected efficiency could be due to the relative dipole alignment of the fluorophores or self-quenching between the fluorophores.

Discussion

The data strongly suggest that our hypothesis is correct: The ensemble conformation of the Nanodyn is sensitive to the presence of macromolecules in solution. However, characterizing this sensitivity and understanding how it relates to the properties of the crowding agent is vital if the Nanodyn is to function as a sensor. For PEG-8000, the Nanodyn has a sensitive range of approximately 1 to 3 mPa*s. At higher viscosities, the sensors are all shut and any difference in viscosity cannot be resolved. The rheology of the cytoplasm has been studied before, and measurements are on the order of 1 mPa*s [35], [36]. This is potentially an ideal use for the Nanodyn as described here. Collagen, a gel and a structural component of the extracellular matrix, has a viscosity on the order of 25 mPa*s, meaning the Nanodyn may require design alterations to enable measurements at higher viscosities [37].

Using the results obtained here, it may be possible to predict the behavior of the Nanodyn in other solutions. If we assume that the Nanodyn and crowding agents are both homogenously distributed in solution, then it is reasonable to suggest that the concentration where all of the Nanodyn are closed is the same as the polymer overlap concentration. The Nanodyn changes configuration due to excluded volume effects – if all of the Nanodyn are closed it must mean there is very little room between crowding agents. Ziębacz et. al. report several measurements of PEG taken at a range of molecular weights and found that the overlap concentration for PEG was related to molecular weight by a power law relationship [38]. Interpolating from their data, the overlap concentration of PEG-8000 is predicted to be 9.7 wt%. This value, corresponding to a viscosity of around 8 mPa*s, is approximately double the point where all of the Nanodyn are closed. We expect that this relationship should be

maintained when other PEG molecules are used as the crowding agent, and this hypothesis will be tested in future work.

Chapter 3: Bulk Viscoelasticity of DNA

Introduction

As a foundation for measuring the viscoelastic properties of DNA origami, we aimed to use shear macrorheology to measure the viscoelastic behavior of dilute DNA solutions. There were several previous publications measuring the rheology of λ-DNA (approximately 42 kilobases) at relatively high concentrations using a rheometer, showing that it was at least plausible to apply the same method for measuring the viscoelastic properties of staple and scaffold DNA [39], [40]. Initial tests focused on measuring the difference in viscoelastic properties at different concentrations of λ-DNA. The goal was to determine optimal testing conditions for smaller, lower concentration DNA samples. Therefore, the strain (oscillation amplitude) and frequency of oscillation were varied. Although the results showed some agreement with literature sources, the bulk rheology results demonstrated some limitations of typical bulk rheology methods. There was no distinguishable difference in the viscoelasticity of dilute samples at differing concentrations. The sample was also subject to evaporation, which made it difficult to run proper experiments. Furthermore, the rheometer required relatively large sample volumes, which would make further tests with DNA origami impractical.

Some background will be given for the use of a rheometer and the literature precedent for measuring the rheology of DNA. The methods used in these experiments will be presented. Finally, the results obtained will be presented and discussed.

Background:

Rheometers and Rheological Testing:

The rheometer is the go-to analytical tool for measuring viscoelastic properties in a variety of viscoelastic fluid samples [41]. Rheometers typically measure shear properties by applying force to a

sample between two parallel plates. The rheometer has two vital components: a motor and a transducer. The motor is required to apply precise deformation to the sample. An accurate rheometer requires a motor that can apply very precise small and large-scale deformations, is very stiff, and has very low run-out (eccentricity between drive shaft and plate). The motor is also coupled with an optical encoder to measure angular displacement. As one of the plates is driven by the motor, the other is held at zero displacement. The force required to maintain the plate at zero displacement is measured by a transducer. State of the art transducers are non-contact and are designed to be infinitely stiff, making them sensitive to micronewton*meter torques. Viscoelastic properties are temperature sensitive, so rheometers also incorporate temperature controllers and sensors. A diagram of a typical rheometer is shown in figure 18, below.

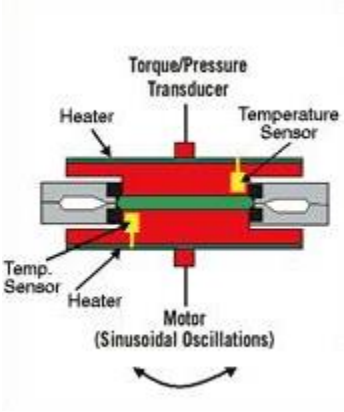

Figure 18: A representative schematic of a parallel plate rheometer. The oscillating motor typically controls the bottom plate, while the top plate senses force. The sample (green) is held between the two plates. Adapted from [42].

Several variables need to be defined to run a test on a rheometer [41]. There are two fundamentally different modes of operation for most rheometers, which are stress controlled and strain controlled, with the latter being more common. In stress-controlled tests, the motor is driven with a given torque, while strain controlled tests apply a specified deformation to the sample. The two tests should theoretically yield identical results, but apparatus design constraints makes it easier to get accurate rheological measurements using strain control. The measurement can also be conducted using

steady shear or oscillatory shear. These two tests measure fundamentally different properties. Steady shear only measures the amount of force required to achieve a certain shear rate, allowing the viscosity to be calculated. For steady shear tests, either the applied torque or the shear rate is specified, while the other quantity is measured. Oscillatory shear allows for the measurement of viscoelastic properties, making it a much more useful test. For oscillatory shear tests, the frequency of oscillation must be specified. Frequency and strain sweeps are common oscillatory shear tests, where frequency or strain is varied while stress is measured.

Rheometers are usually designed to accommodate a variety of plate geometries. Parallel plates are common, but cone-plate and couette geometries are also common (Figure 19).

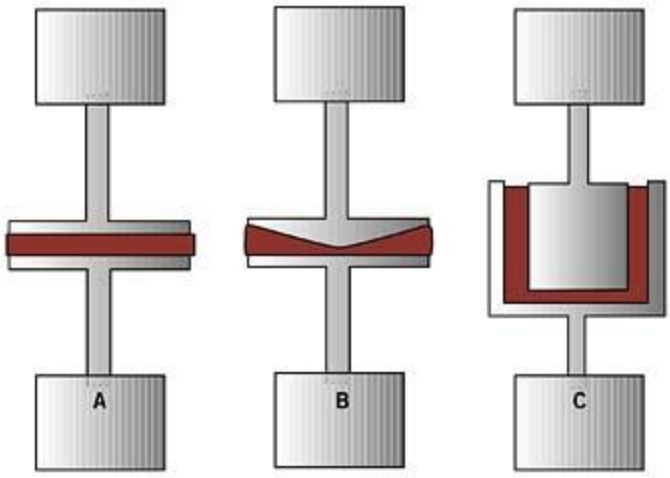

Figure 19: Common rheometer geometries: parallel plates (A), cone and plate (B), couette (C). Adapted from [43].

Although the geometries are different, they all have the same operating principle: stress is calculated from the force measured by the transducer and the contact area. Different geometries have different areas and different sample size requirements, and apply force in different ways. Parallel plates are simple, require relatively small sample sizes (1-2 ml), and the gap between them can be altered. However, due to the change in velocity from the center to the edge of the plate, there is variation in the shear rate. Cone-plate geometries provide move with a constant shear rate, but have a non-constant

gap size. Couette geometries greatly increase the contact area between the instrument and the sample, increasing the accuracy of measurements at low viscosity. However, these geometries require large sample volumes and have larger moments of inertia, making them incompatible with shear rate changes or high oscillation frequency.

Viscoelasticity of DNA

There has been considerable interest in the viscoelastic properties of DNA for several years, and various papers have been published on the topic. Mason et al. used 13 kbp calf thymus (CT) DNA over a concentration range from 1 mg/ml to 10 mg/ml to measure the rheology of semi-dilute and entangled DNA [44]. They first report strain sweeps at a range of concentrations from .01 radians to 10 radians at 1 rad/s and frequency sweeps from .1 rads/s to 43 rad/s at a strain of .02. They found that at low strain conditions corresponding to linear viscoelasticity, G' and G'' are not functions of strain and increase with concentration. Their results suggest that it might be possible to differentiate between different concentrations of DNA that represent different stages in the DNA origami folding process.

Another group reported the intrinsic viscosity of small DNA duplexes (20-395 bp) using capillary viscometry, a low-shear viscosity measurement method that measures the time it takes for a solution to fall through a narrow tube [45]. Intrinsic viscosity is a measure of the viscosity contributions of a molecule in solution independent of the solvent viscosity. It is calculated in the limit of zero concentration, so it cannot be used to predict viscosity based on concentration. Based on their report, intrinsic viscosity increases by approximately 50 times for dsDNA from 20 bp to 395 bp. They also found that there is no non-Newtonian viscoelastic behavior in dilute double stranded DNA below approximately 1000 base pairs.

Finally, a study published in August 2016 by Bravo-Anaya et. al. studied the viscoelastic properties of DNA strands at a range of lengths and concentrations [46]. They found that the overlap

concentration for short DNA strands is very high, around 125 mg/ml. They also determined that short DNA strands are typically not viscoelastic.

Methods

Rheological experiments were conducted to measure the viscoelastic properties of the DNA particularly related to DNA origami. The scaffold is present in a typical folding reaction at 20 nM with staples at 200 nM. Given the known length of the scaffold and the approximate length and amount of staples, folding reactions are at approximately 1 mg/ml of total DNA. Staples and scaffold are both relatively expensive and hard to produce at volumes applicable to bulk rheology, so viscoelasticity in other types of DNA was explored first. λ-DNA ("lambda DNA") is a 42 kbp linear DNA duplex, which is isolated from a bacteriophage. λ-DNA has many applications in molecular biology and can be purchased in high concentrations relatively cheaply. CT-DNA is another common biological reagent. Large single stranded DNA molecules are isolated and sheared to generate a homogeneous but polydisperse solution DNA with an average length of approximately 2 kbp. The rheology of both λ-DNA and CT-DNA has been studied extensively, and both are much cheaper than scaffold or staples molecules, so initial rheological tests were performed on these solutions.

Rheological Measurements

Solutions of λ-DNA and CT-DNA were diluted in their respective storage buffers to the desired concentration. λ-DNA was suspended in 1X TE buffer (10 mM tris-HCl, 1 mM EDTA) while CT-DNA was suspended in ddH_2O. An ARES G2 rheometer in Dr. Kurt Koelling's lab was used to conduct bulk rheological measurements. Parallel plates (Diameter = 25 mm) were used for all tests. Initially, the experimental goal was to determine the ideal testing conditions for dilute DNA, so frequency and strain sweeps were conducted. For frequency sweeps, the strain was held constant at 1, 10, or 100 radians

while strain rate was varied from 0.1 to 100 rad/s. For strain sweeps, the frequency was held constant at 1, 10, or 100 rad/s while the strain was varied from .1 to 500 radians. The upper limit on strain was governed by the ability of the rheometer to accurately rotate the plate.

To actually perform measurements, a sample was transferred from an epi tube to the plate using a pipette. The sample was pipetted up and down several times to mix it before transfer. Approximately 1 ml of sample was added to the plate, although the volume was not precisely controlled. The constraint on volume was related to the size of the plate – ideally, the gap between plates was between 1 and 2 mm, corresponding to a volume between 0.5 and 1 ml. After loading the sample, the top plate was lowered towards the bottom until the top plate touched the sample. The top plate was then very slowly lowered until the sample formed a uniform column. A test was then conducted over a time span of 1 to 5 minutes. The total time was a function of the frequencies and strains involved in the test. After a test was conducted, the gap was narrowed slightly to account for evaporation before another test was conducted. After all tests had been run on a given sample, the remaining sample was collected using a pipette and used in later experiments.

Results

The results of identical strain sweeps at several λ-DNA concentrations are shown in figure 20, below. The strain sweeps were conducted from .05 radians to 500 radians at a frequency of 1 rad/s.

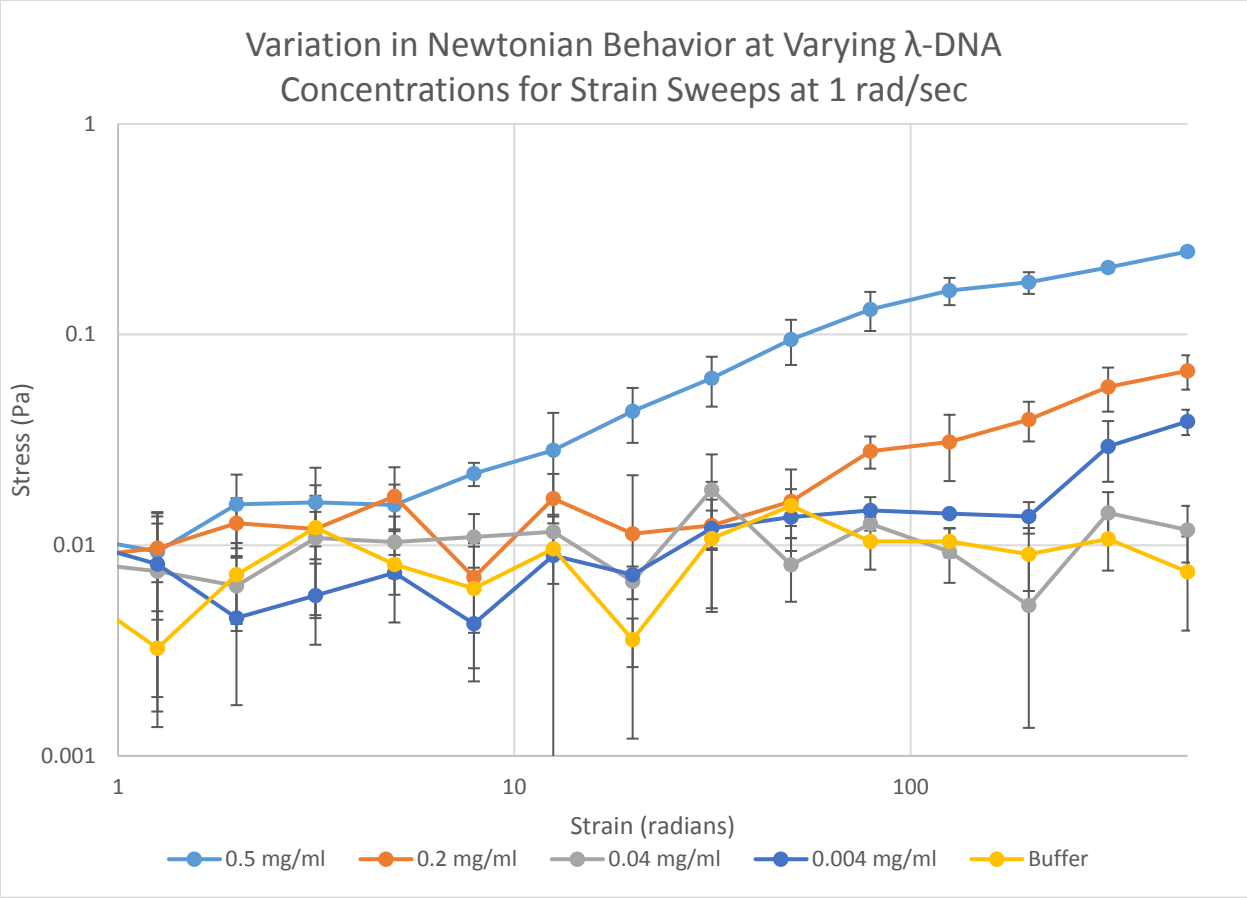

Figure 20: The results of changing DNA concentration on the stress-strain relationship of the solution. Newtonian fluids have a constant linear stress-strain relationship. A decrease in slope is indicative of shear thinning. Error bars represent one standard deviation based on three replicates.

There are several obvious observations from figure 20. First, higher DNA concentrations require more force to deform for a given strain and therefore are more viscous. This is both intuitively and theoretically expected. The figure also shows deviations from Newtonian behavior at the highest concentration. The correlation between stress and strain in Newtonian fluids should be linear and constant. At 0.5 mg/ml concentration, the slope decreases at higher strain. This non-Newtonian behavior is known as shear thinning and is characteristic of linear polymers. As the polymer is deformed, they stretch to a more linear conformation and require less force to deform further, leading to the observed decrease in viscosity. This is also dependent on the shear rate.

Figure 20 also gives some insight to the resolution of the rheometer. The required stress and corresponding viscosity decrease with concentration, but the ability to distinguish between concentrations based on the rheological measurements shown here is tenuous at best below 0.2 mg/ml. DNA origami folding reactions contain 0.05 mg/ml large scaffold and 0.45 mg/ml short staples, for about 0.5 mg/ml total DNA. However, the staples are in 10x excess and only 10% of them will bind with the scaffold under ideal conditions. Therefore, the rheometer ideally needs to detect viscoelastic differences between solutions in the μg/ml range.

There was also evidence of viscoelasticity in λ-DNA, as is shown by the changing elastic and viscous moduli shown in strain sweeps. The following figure, from reference 44, shows how viscoelasticity is effected by strain in long (13 kbp) DNA strands. The DNA studied in figure 21 has an overlap concentration of approximately 0.7 mg/ml, so the range of values tested are all above the entanglement concentration of the DNA.

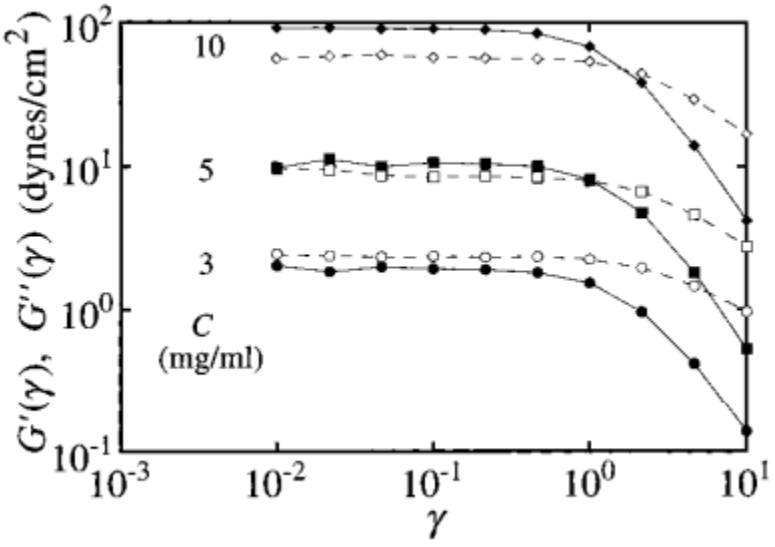

*Figure 21: Plot of G' and G'' of 13 kbp DNA strands measured in an oscillatory strain sweep on a shear rheometer. Solid symbols are for G', while open symbols are G''. The oscillatory frequency was fixed at 1 rad/s. 1 dyne/cm² is equivalent to 0.1 Pa*s. Modified from [44].*

Figure 21 serves as a reference for the strain sweep tests conducted here on λ-DNA. The concentration of λ-DNA used varied from 0.004 mg/ml to 0.5 mg/ml. Calculations indicate that the overlap concentration of λ-DNA should be approximately 0.25 mg/ml, so viscoelastic behavior should be prominent above this concentration in the samples studied here. A plot of the viscous and elastic moduli (Figure 22) show this to be the case.

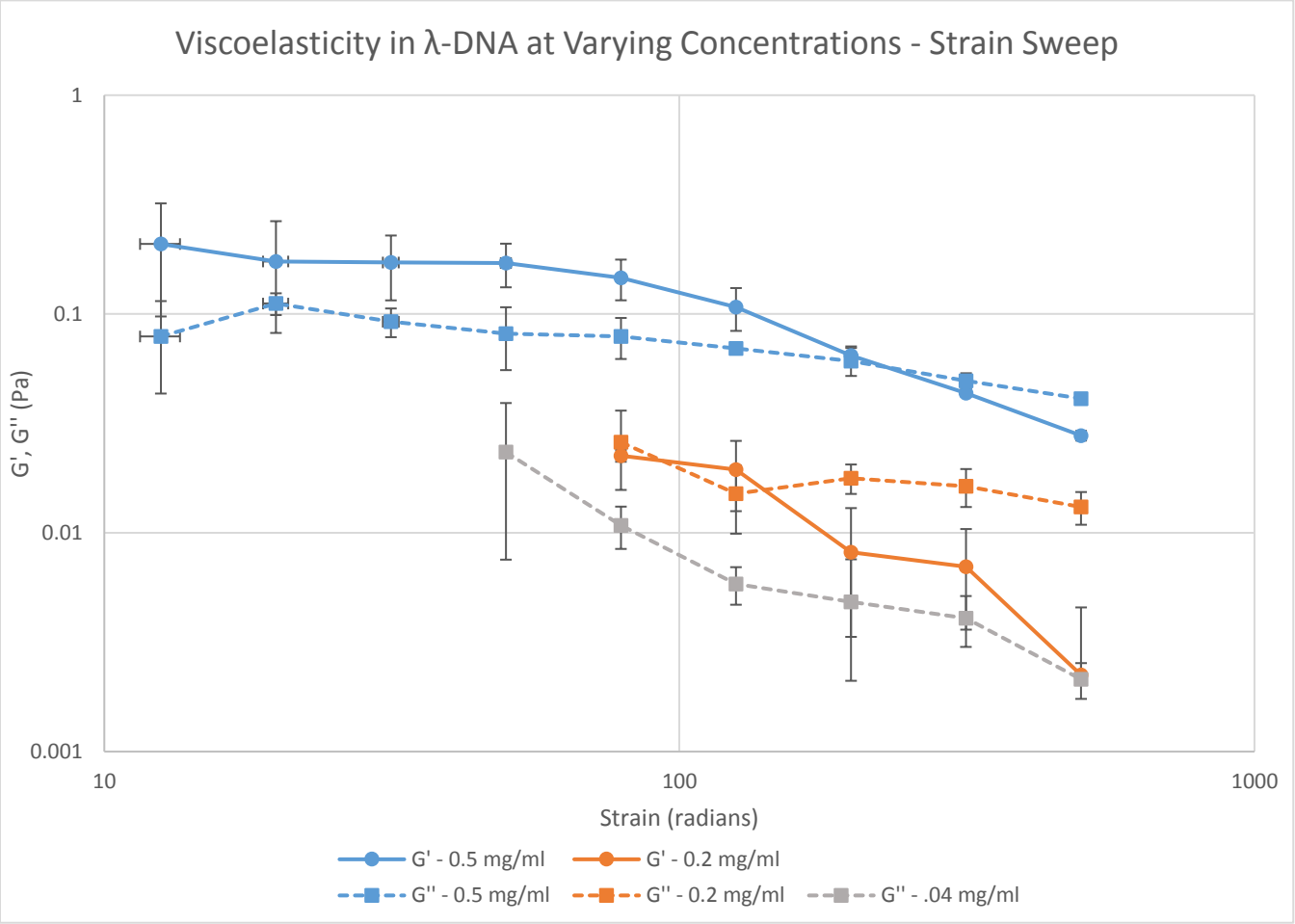

Figure 22: Viscoelastic Moduli from strain sweep of λ-DNA at varying concentration. The data show a decrease in the storage and loss moduli as concentration is decreased. Noise in the measurement prevented data from lower concentrations being added. Error bars represent 1 standard deviation based on 3 replicates.

Figure 22 shows how the storage and loss moduli changed with increasing strain at different concentrations. The measurements were noisy, especially at low concentrations and strains, to the point that the data was omitted from the plot. However, the data shown agrees qualitatively with the data

shown in figure 21. At the highest concentration, a plateau in G’ and G’’ is observed at low strain around .1 Pa, with G’ dominating. The plateau drops off around 100 radians, with G’’ starting to dominate at the crossover strain of 250 radians. Although the plateau moduli are not observed in the 0.2 mg/ml sample, there appears to be a crossover strain between 80 and 125 radians, less than the value for the higher concentration. Finally, the magnitude of both moduli dropped with concentration. All of these results agree with theory and with other studies, and confirm that solutions of large DNA strands are viscoelastic. However, the applicability of the λ-DNA tests is questionable because λ-DNA is much longer than either the scaffold or the staple molecules currently used in DNA origami, and viscoelastic properties are strong functions of polymer length.

CT-DNA solutions were also studied using bulk rheometry. Higher concentrations were able to be studied due to the stock concentration of CT-DNA. However, the data in general was noisier for CT-DNA due to the much shorter chains. For instance, the results of stress-strain relationship of three separate strain sweeps, each replicated three times total, can be seen in the following figure.

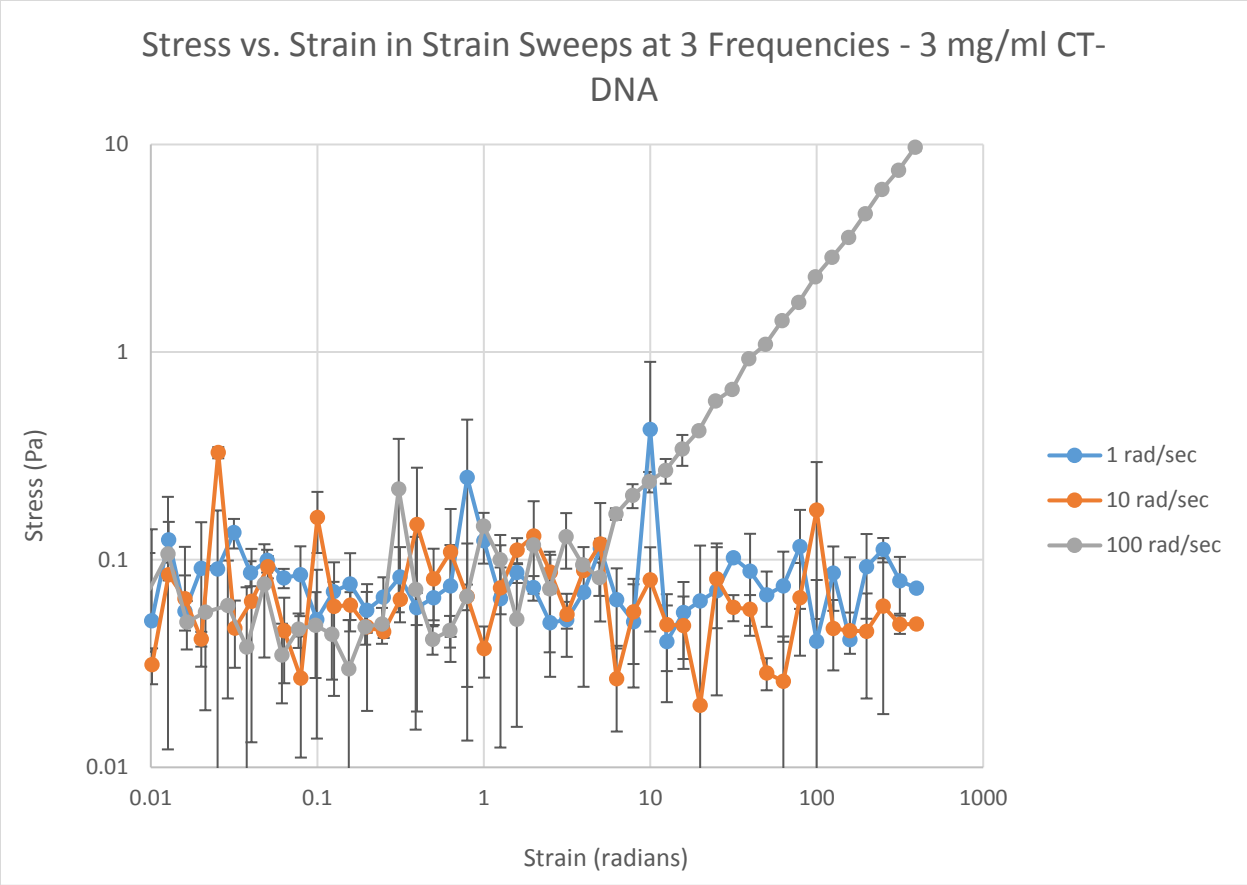

Figure 23: Average stress vs strain for triplicate strain sweeps of 3 mg/ml CT-DNA at 3 frequencies. Both 1 rad/sec and 10 rad/sec were very noisy, and no signal was detected at 100 rad/sec at low strain.

The data show that it is impossible to measure stress at low frequencies, even for relatively highly concentrated DNA. However, it also shows that there is no distinguishable shear-thinning in the short DNA strands studied here. There are two interpretations for this behavior. The shorter DNA strands could be so small that they are essentially rigid on the scale of shear forces relevant to this work and do not change orientation appreciably when shear is applied. Alternatively, they could be capable of the same non-Newtonian behavior that was observed in longer DNA. However, given that the individual molecules are shorter, unaligned particles experience less drag and therefore take longer to align. This second possibility is in agreement with literature.

The elastic and viscous moduli of CT-DNA support the previous observation that measuring the viscoelasticity of short DNA strands using a bulk rheometer may be difficult (Figure 24). There was no discernible pattern in either G' or G'' as a function of CT-DNA concentration.

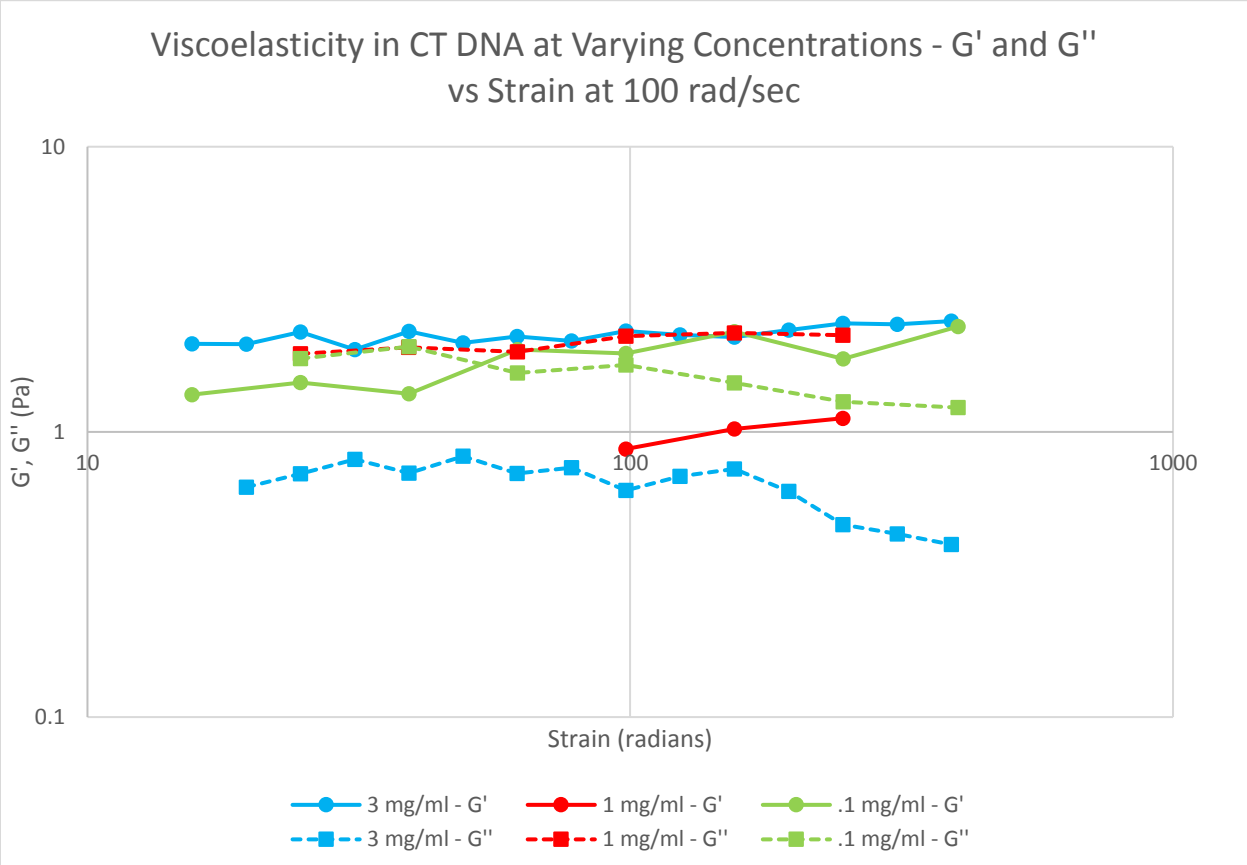

Figure 24: Comparison of viscoelastic moduli in CT-DNA at varying concentrations. The data is very noisy, and it appears as though the elastic and viscous moduli are constant over the range of strains studied here.

Figure 24 shows that the elastic and viscous moduli depend very little on strain, indicating that the material is linearly viscoelastic in this range of strains.

Discussion

These tests show that DNA can be studied as a polymer. It has polymeric viscoelasticity and undergoes shear thinning. These factors are crucial for understanding fundamental biophysical

questions. For instance, DNA organization in the nucleus is fundamentally related to the stiffness of the DNA helix and other rheological factors. The structure of polymers is also fundamentally related to transport properties in polymer solutions, meaning that an improved understanding of DNA polymer dynamics could improve our understanding of the influence of regulatory molecules which work in the nucleus.

The results here do not support the hypothesis that DNA origami folding can be studied using bulk rheology. Based on the data gathered from these experiments, there are two independent conclusions which can be drawn. First, the origami staples, which make up 90% of the DNA in solution, are not appreciably viscoelastic. Second, it is unlikely that the rheometer used here will be able to detect the extremely subtle changes in material properties that should accompany DNA origami folding. One possibility would be to improve some of the control or measurement elements on the rheometer, but the noise associated with the samples that were tested in these experiments was substantial and probably will not be remedied by incrementally improved transducers or motors.

There are also several problems inherent to the method that suggest it is not applicable for DNA origami. Firstly, there is the problem of evaporation. As the sample sits between the rheometer plates, it is constantly evaporating. Slight evaporation can be accounted for by changing the plate gap. It can also be mitigated by isolating the rheometer plates and adding a solvent trap to the chamber. The solvent trap controls the humidity in the chamber and slows the rate of evaporation, but it remains a nuisance variable. More importantly, the sample size requirements for bulk rheology are almost certainly prohibitive. Neither scaffold nor staples are cheap, and the sample size and concentration requirements for a rheological measurement are both much larger than is typical for DNA origami folding.

Chapter 4: Microrheology of DNA

Viscoelasticity is generally a property of the molecular scale structure and interactions in a material. Rheometers probe this structure by measuring the bulk material response to imposed force, but they are not the only measurement method. Microrheology in general refers to the variety of methods that measure the rheology of a substance by studying the behavior of microscopic particles suspended in that substance. Microrheological experiments have many benefits compared to experiments conducted on a rheometer. For one, they require very small samples – on the order of 10 µl. They also allow for the characterization of materials at different length scales, something that bulk rheology cannot do.

Background

Microrheology relies on the connection between two derivations for the diffusivity of a particle in a viscous solution. Here we present the mathematical background of microrheology. It also involves the use of particle tracking hardware and software. Video microscopy will be introduced, along with the workflow for extracting rheological measurements from videos.

The Mathematics Behind Particle Diffusion

Particle tracking microrheology relies on two separate equations that predict the behavior of molecules or particles experiencing Brownian motion. One of these, the Stokes-Einstein relationship, is derived from first principles based on the collisions experienced by the bead. The other expression is derived from Fick's law and the assumption that the bead diffuses randomly through a material.

In 1905, Einstein published his dissertation on the motion of particles [47]. He showed that the diffusion of a bead in solution was a function of only temperature and the shape of the bead. He derived an expression for the diffusivity of a bead that was a function of bead shape and temperature:

$$D = \frac{k_B T}{\xi} \tag{12}$$

Where D is particle diffusivity, also referred as the diffusion constant, and ξ is a friction factor for the particle representing the ratio of particle velocity to drag force in solution. The friction factor for a spherical bead is given by Stokes law [48]:

$$\xi = 6\pi\eta r \tag{13}$$

where η is the solution viscosity and r is the particle radius. Stokes law is valid for small particles at low Reynolds numbers. The Stokes-Einstein equation for bead diffusivity is therefore:

$$D = \frac{k_B T}{6\pi\eta r} \tag{14}$$

The diffusion of a particle can also be derived independently from continuum mass transport using Fick's law and conservation of mass [49]. 1-dimensional diffusion can be used as a representative derivation. Diffusion in 1-D is governed by the following equation:

$$\frac{\partial c}{\partial t} = D\frac{\partial^2 c}{\partial x^2} \tag{15}$$

For a concentration of c_0 at a position of x=0 at time t = 0, the concentration profile at a future time t is given by:

$$c(x,t) = \frac{N}{\sqrt{4\pi D t}} * \exp\left(-\frac{x^2}{4Dt}\right) \tag{16}$$

$$N = \frac{c_0(x)}{\delta(x)}\ at\ t = 0 \tag{17}$$

N is the total number of particles in the sample, which are assumed to be placed at x=0 at the initial time.

Equation 16 describes how the distribution of particles will spread out over time, but it can also be thought of as a probability distribution for finding an individual particle at location x and time t. Specifically the probability of finding a particle in an infinitesimally small slice of the x-axis is based on the total amount of particles and their initial concentration:

$$P(x)dx = \frac{c(x)}{N}dx \tag{17}$$

The expectation value for the position of a particle in 1-D diffusion is given by:

$$\langle x^2 \rangle = \int_{-\infty}^{\infty} x^2 * P(x)dx \tag{18}$$

$$\langle x^2 \rangle = \int_{-\infty}^{\infty} \frac{x^2}{\sqrt{4\pi Dt}} \exp\left(-\frac{x^2}{4Dt}\right) dt \tag{19}$$

$$\langle x^2 \rangle = 2Dt \tag{20}$$

The expected value of a particle in 1-D diffusion is a function of time and the diffusivity of the particle. The equipartition theorem shows that the constant multiple is a function of the dimension; it is four for 2-D diffusion and six for 3-D diffusion. The root-mean-square displacement of a particle in 2-D diffusion is then:

$$x_{RMSD} = \sqrt{4Dt} \tag{21}$$

Two equations have been derived which relate to the diffusivity of a particle in viscous media at low Reynolds numbers. The goal is still to measure viscoelastic properties of solutions, so combining those expressions (equations 21 and 14) and solving for viscosity yields:

$$\eta = \frac{k_B T}{6\pi r} * \frac{4t}{\langle x_{RMSD} \rangle^2} \tag{22}$$

Using that equation, the viscosity of a solution can be calculated if several variables are known. Temperature can be measured easily. Microscale beads can be purchased which will satisfy all of the conditions for Stokes drag, and the radius of these beads should be known. If the Root mean squared displacement of the bead can be measured over time, the solution viscosity can be calculated. The method described here can be used for calculating pure viscosity, but it can be extended to measure viscoelastic properties by calculating the frequency dependence of bead displacements [50].

Particle Tracking

In order to calculate the bead RMSD, video microscopy and particle tracking algorithms are used. Video microscopy is essentially the capture of microscopic images with a high framerate, but the details of implementation may vary. For microrheology, the video microscopy system needs to be able to capture images with high enough resolution to differentiate between beads as small as 100 nm in diameter. Depending on the application, using fluorescence to excite fluorophores on the surface of a bead may improve image quality. For instance, a thick polymer network might interfere with following the trajectory of a bead using bright-field microscopy, but fluorescence may allow the particle to be tracked.

After bead motion has been captured on video, frame by frame image processing can extract the trajectory. There are several general steps a particle tracking algorithm must follow. The video frames the tracking algorithm takes in are given thresholds, meaning that any pixel above a certain value is set to black and any pixel below a certain value is set to white. A bandpass filter is used to remove high-frequency noise from the image. The particles can then be identified in the processed image.

Some particle tracking algorithms have automatic particle identification, but the method used here relied on human input of a particle location in the first video frame. After manual location selection the next frame in the video was processed identically. Based on the location of the particle in the

previous frame, the location of the maxima nearby that location in the current frame, and the distribution of intensities around the maxima, the particle position is determined in this frame. The algorithm is repeated for each frame in the video until the end is reached. In this way, particle position can be tracked over time. The resulting trajectory can be analyzed to extract the root mean square of position.

Methods

To prepare a microrheological experiment, a sample had to be prepared. The sample then had to be imaged, and the resulting images had to be processed and analyzed to extract particle trajectories.

Sample Preparation

To prepare a sample, 5 µl of fluorescent bead suspension was vortexed and combined with the desired sample at 2X concentration in a 1:1 ratio. The fluorescent beads had a nominal radius of 0.5 µm and fluoresced under 561 nm light. The fluorescent bead stock was mixed at a volume fraction of 10^{-4} beads. After the beads were added to the sample, 5 µl of the sample was added to a slide and a 22mm x 22mm glass coverslip was applied to the solution. Compressed air was used to remove dust from both the slide and the coverslip. After the sample had spread under the coverslip, the coverslip was moved to ensure that no air bubbles were present in the sample and that the sample was evenly distributed. Nail polish was applied at the edge of the slide and allowed to dry in order to seal it.

Microscopy and Image Processing

A Nikon eclipse Ti-E total internal fluorescence microscope (TIRF) system was used to image the fluorescent beads in TIRF mode. The beads were excited using a 561 nm laser. AVI video was acquired at multiple locations on the slide. Videos were typically taken over ten seconds at 30 frames per second and a magnification of 100x. Locations were ideally selected that had several beads in frame to minimize image processing.

After video was recorded it was processed using a MATLAB script. After images had been processed with MATLAB, the trajectories were examined and compared with the video footage. Occasionally, particles would leave the focal plane of the microscope during the video, leading to aberrant trajectories. These trajectories were discarded and the mean square displacement of each particle was calculated from the remaining trajectories. The average particle displacement was the calculated and the particle diffusivity was fit using equation 22.

Results

The initial goal of microrheological tests was to validate the method. Therefore, the viscosity of water was measured first. By using the TIRF microscope, video footage was taken of bead diffusion which was able to be processed by the MATLAB particle tracking algorithm described previously. A sample frame from a video is shown in figure 25.

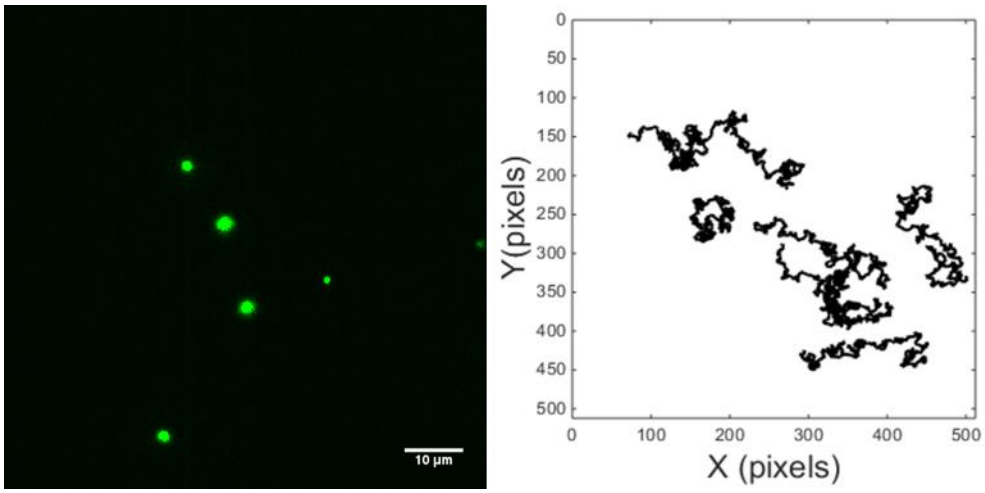

Figure 25: Left: Representative frame of a microscopy video used for particle tracking. Right: Trajectories aquired from MATLAB particle tracking script.

After capturing several videos, the trajectories of particles were analyzed in MATLAB. The resulting trajectories and RMSD can be seen in the following figure (figure 26).

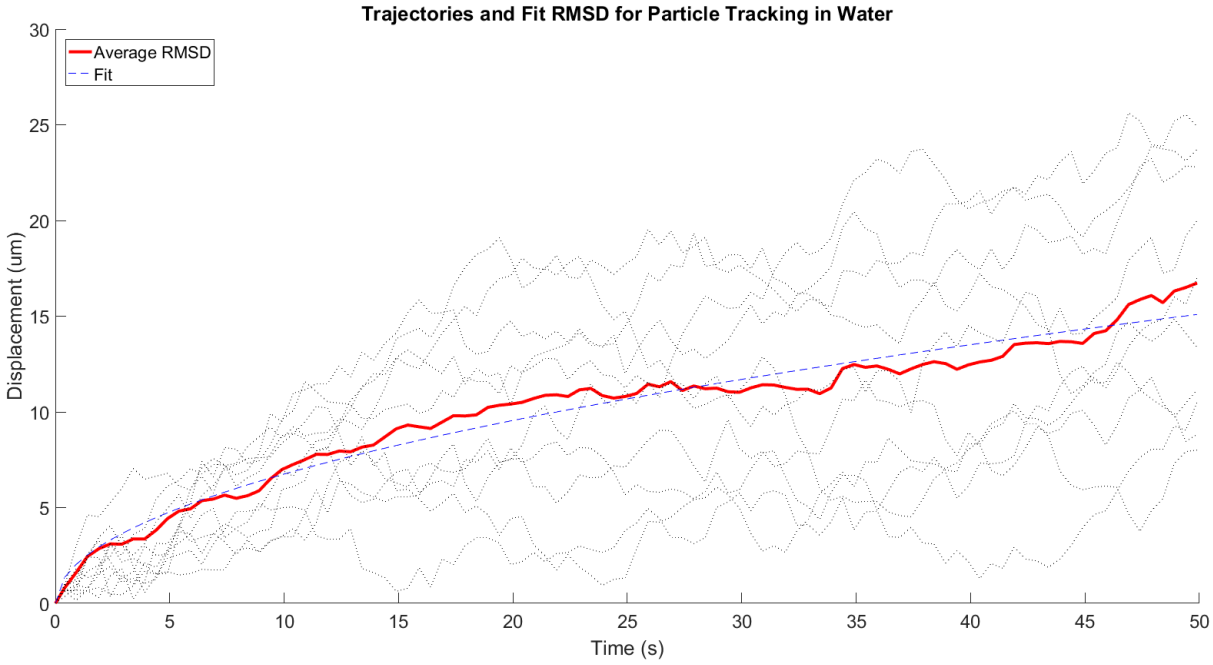

Figure 26: The trajectory of ten tracked beads is shown. In the picture above, the particle was tracked over 50 seconds. The displacement shown corresponds to a diffusivity of 2.28 $\mu m^2/sec$.

Initial tests using particle tracking microrheology show that the viscosity of water and glycerol can be calculated. The results are shown in figure 27.

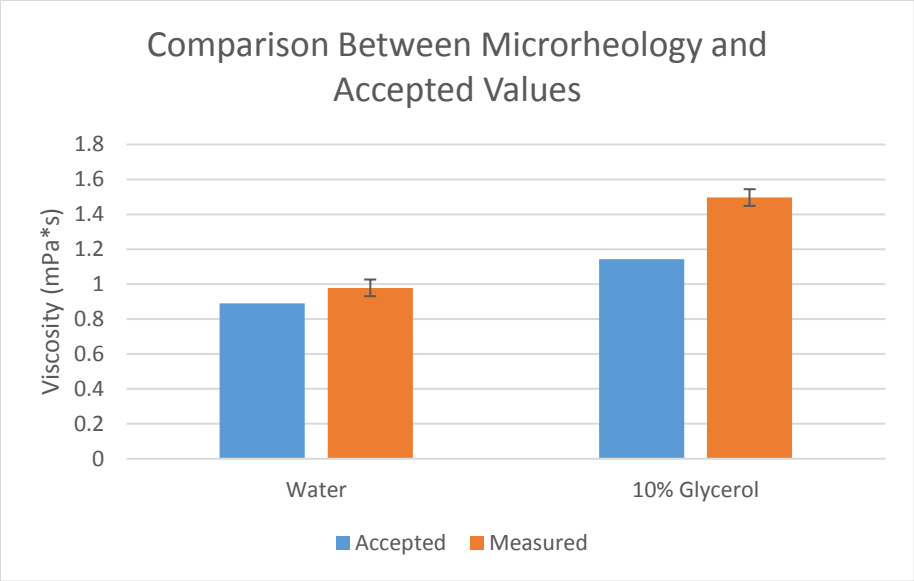

Figure 27: The difference between accepted literature values and measured values for the viscosity of water and 10% glycerol.

Clearly, the microrheological tests need to be improved significantly before they will be a feasible replacement for bulk rheology. However, there are several potential causes for the deviation in measured viscosity. Firstly, the particles could be close to the surface of the slide, meaning their motion is not totally Brownian. This would slow the particles, leading to a decrease in measured diffusivity and a resulting increase in viscosity. Modifications to slide prep, such as sandwiching the sample between pieces of double sided tape to make a wider channel, could be effective.

Discussion

Quantitatively, the data gathered here leaves a lot to be desired. However, several examples from literature suggest that this method is worth pursuing. This preliminary work did show that diffusivity can be measured and validated the general workflow. With further optimization and literature review, the method should provide much more accurate measurements of viscosity.

There are several reasons to think that the method is both applicable to DNA origami and worth pursuing over macrorheology. The small sample size required is very attractive. Similar particle tracking methods can allow for the measurement of viscoelastic properties beyond simple viscosity. Taking the

Fourier transform of the RMSD trajectory yields a power spectrum, which allows for the calculation of G' and G''. This mathematical technique is commonly combined with optical trapping microrheology, which measures the position deviations for a bead held in place by an optical trap. Optical trapping requires more equipment than basic particle tracking microrheology, but it is a well-established technique.

The method can also yield measurements that are fundamentally unobtainable using macrorheology. Bulk macrorheology measures how the sample as a whole dissipates and stores force. On the other hand, microrheology is sensitive to length scales within the sample, and different viscoelastic characteristics can be measured by probing the system in different ways. Liu et. al. use microrheology to measure viscoelasticity in actin networks of varying average filament lengths [51]. They found that studying the correlation of diffusion for two distant particles gave measurements that were in agreement with bulk rheology and constant with varying filament length. They also measured the diffusivity of single particles, and found that single particle diffusivity was correlated with actin length. The correlation of two particles is a result of longer timescale interactions in the actin network, which single particle microrheology is not sensitive to. Differentiating between the material behavior at these length scales may be useful for the study of DNA origami. Given that the individual DNA molecules are packed relatively tightly upon folding, there would be very little long distance correlation between the diffusion of particles after folding.

Conclusions and Future Work

The overall objective of this thesis was to explore the connection between microscale structural characteristics of materials and their macroscale behavior in the context of DNA origami. Chapter one presented preliminary results that demonstrate the use of DNA origami for measuring rheological behavior. If the Nanodyn can be fully characterized, it should be able to provide valuable biophysical information.

Future work will focus on three primary aspects of the Nanodyn. Firstly, the response of the Nanodyn will be measured using a variety of crowding agents. We hypothesize that the structure of the crowding agent should determine how it affects the Nanodyn. Further, because DNA is charged the charge, polarity, and other chemical properties of the crowding agent will mediate the Nanodyn response. In order to take quantitative measurements using the Nanodyn, all of these effects must first be quantified. Along with variations in crowding agent, variations in the Nanodyn will also be explored. As shown in figure 11, each linker can be constrained individually. The energetic interactions of the fluctuating linker can also be modified by changing the staple length. If these factors are quantified, the useful range of the Nanodyn may be increased. Finally, the design of the Nanodyn may be modified. Changing the size of the barrel or the gap between barrels should change the sensitivity of the device.

The rheology of DNA also warrants further study. Although measuring viscoelastic changes as folding progresses may not be realistic, there are several interesting questions that rheology could help answer. For instance, we have found that molecular crowding can inhibit DNA origami folding. An experiment was performed The experiment showed that structure folding completely stopped above a certain concentration – possibly because solution viscosity inhibited staple diffusion.

To answer questions relating to viscoelasticity and DNA origami, work should focus on the development and improvement of microrheology. A full factorial experiment for particle size and

surface chemistry could be performed to ensure that particles are compatible with DNA. The results of the experiment should be confirmed using bulk rheology. Potentially the optical trap we have could be calibrated, allowing viscoelastic measurements of DNA to be conducted. Ideally, an experimental procedure and setup allowing for the determination of DNA viscoelasticity will be produced.

Bibliography

[1] L. Pray, “Discovery of DNA Structure and Function: Watson and Crick,” *Nat. Educ.*, vol. 1, no. 100, 2008.

[2] J. D. Watson and F. H. Crick, “Molecular structure of nucleic acids; a structure for deoxyribose nucleic acid,” *Nature*, vol. 171, no. 4356, pp. 737–738, Apr. 1953.

[3] P. Yakovchuk, “Base-stacking and base-pairing contributions into thermal stability of the DNA double helix,” *Nucleic Acids Res.*, vol. 34, no. 2, pp. 564–574, Jan. 2006.

[4] N. C. Seeman, “Nucleic acid junctions and lattices,” *J. Theor. Biol.*, vol. 99, no. 2, pp. 237–247, Nov. 1982.

[5] P. W. K. Rothemund, “Folding DNA to create nanoscale shapes and patterns,” *Nature*, vol. 440, no. 7082, pp. 297–302, Mar. 2006.

[6] S. M. Douglas, H. Dietz, T. Liedl, B. Högberg, F. Graf, and W. M. Shih, “Self-assembly of DNA into nanoscale three-dimensional shapes,” *Nature*, vol. 459, no. 7245, pp. 414–418, May 2009.

[7] C. E. Castro *et al.*, “A primer to scaffolded DNA origami,” *Nat. Methods*, vol. 8, no. 3, pp. 221–229, Mar. 2011.

[8] X. Wei, J. Nangreave, and Y. Liu, “Uncovering the Self-Assembly of DNA Nanostructures by Thermodynamics and Kinetics,” *Acc. Chem. Res.*, vol. 47, no. 6, pp. 1861–1870, Jun. 2014.

[9] H. Li, T. H. LaBean, and K. W. Leong, “Nucleic acid-based nanoengineering: novel structures for biomedical applications,” *Interface Focus*, vol. 1, no. 5, pp. 702–724, Oct. 2011.

[10] J. Bath, S. J. Green, K. E. Allen, and A. J. Turberfield, “Mechanism for a Directional, Processive, and Reversible DNA Motor,” *Small*, vol. 5, no. 13, pp. 1513–1516, Jul. 2009.

[11] S. M. Douglas, I. Bachelet, and G. M. Church, “A logic-gated nanorobot for targeted transport of molecular payloads,” *Science*, vol. 335, no. 6070, pp. 831–834, Feb. 2012.

[12] A. Kuzuya, R. Watanabe, Y. Yamanaka, T. Tamaki, M. Kaino, and Y. Ohya, “Nanomechanical DNA Origami pH Sensors,” *Sensors*, vol. 14, no. 10, pp. 19329–19335, Oct. 2014.

[13] P. D. Halley *et al.*, “DNA Origami: Daunorubicin-Loaded DNA Origami Nanostructures Circumvent Drug-Resistance Mechanisms in a Leukemia Model (Small 3/2016),” *Small*, vol. 12, no. 3, pp. 307–307, Jan. 2016.

[14] Q. Zhang *et al.*, “DNA Origami as an *In Vivo* Drug Delivery Vehicle for Cancer Therapy,” *ACS Nano*, vol. 8, no. 7, pp. 6633–6643, Jul. 2014.

[15] J. Song *et al.*, “Isothermal Hybridization Kinetics of DNA Assembly of Two-Dimensional DNA Origami,” *Small*, vol. 9, no. 17, pp. 2954–2959, Sep. 2013.

[16] A. E. Marras, L. Zhou, V. Kolliopoulos, H.-J. Su, and C. E. Castro, “Directing folding pathways for multi-component DNA origami nanostructures with complex topology,” *New J. Phys.*, vol. 18, no. 5, p. 55005, May 2016.

[17] C. Bouchiat, M. D. Wang, J.-F. Allemand, T. Strick, S. M. Block, and V. Croquette, “Estimating the Persistence Length of a Worm-Like Chain Molecule from Force-Extension Measurements,” *Biophys. J.*, vol. 76, no. 1, pp. 409–413, Jan. 1999.

[18] L. Zhou, A. E. Marras, C. E. Castro, and H.-J. Su, “Pseudorigid-Body Models of Compliant DNA Origami Mechanisms,” *J. Mech. Robot.*, vol. 8, no. 5, p. 51013, May 2016.

[19] P. E. Rouse, “A Theory of the Linear Viscoelastic Properties of Dilute Solutions of Coiling Polymers,” *J. Chem. Phys.*, vol. 21, no. 7, p. 1272, 1953.

[20] M. O. Steinhauser and S. Hiermaier, “A Review of Computational Methods in Materials Science: Examples from Shock-Wave and Polymer Physics,” *Int. J. Mol. Sci.*, vol. 10, no. 12, pp. 5135–5216, Dec. 2009.

[21] Q. Ying and B. Chu, “Overlap concentration of macromolecules in solution,” *Macromolecules*, vol. 20, no. 2, pp. 362–366, Mar. 1987.

[22] D. Marenduzzo, K. Finan, and P. R. Cook, “The depletion attraction: an underappreciated force driving cellular organization,” *J. Cell Biol.*, vol. 175, no. 5, pp. 681–686, Dec. 2006.
[23] D. Miyoshi and N. Sugimoto, “Molecular crowding effects on structure and stability of DNA,” *Biochimie*, vol. 90, no. 7, pp. 1040–1051, Jul. 2008.
[24] Q. Mei *et al.*, “Stability of DNA Origami Nanoarrays in Cell Lysate,” *Nano Lett.*, vol. 11, no. 4, pp. 1477–1482, Apr. 2011.
[25] M. Hudoba, “Force Sensing Applications of DNA Origami Nanodevices,” Ph.D Dissertation, The Ohio State University, Columbus, Ohio, 2016.
[26] K. R. Levental *et al.*, “Matrix Crosslinking Forces Tumor Progression by Enhancing Integrin Signaling,” *Cell*, vol. 139, no. 5, pp. 891–906, Nov. 2009.
[27] A. E. Marras, L. Zhou, H.-J. Su, and C. E. Castro, “Programmable motion of DNA origami mechanisms,” *Proc. Natl. Acad. Sci.*, vol. 112, no. 3, pp. 713–718, Jan. 2015.
[28] T. Förster, “Energy migration and fluorescence,” *J. Biomed. Opt.*, vol. 17, no. 1, p. 11002, 2012.
[29] R. Roy, S. Hohng, and T. Ha, “A practical guide to single-molecule FRET,” *Nat. Methods*, vol. 5, no. 6, pp. 507–516, Jun. 2008.
[30] P. Held, “An Introduction to Fluorescence Resonance Energy Transfer (FRET) Technology and its Application in Bioscience,” 2012.
[31] E. Stahl, T. G. Martin, F. Praetorius, and H. Dietz, “Facile and Scalable Preparation of Pure and Dense DNA Origami Solutions,” *Angew. Chem.*, vol. 126, no. 47, pp. 12949–12954, Nov. 2014.
[32] R. M. Clegg, “Fluorescence resonance energy transfer and nucleic acids,” *Methods Enzymol.*, vol. 211, pp. 353–388, 1992.
[33] P. Gonzalez-Tello, F. Camacho, and G. Blazquez, “Density and Viscosity of Concentrated Aqueous Solutions of Polyethylene Glycol,” *J. Chem. Eng. Data*, vol. 39, no. 3, pp. 611–614, Jul. 1994.
[34] F. Han, J. Zhang, G. Chen, and X. Wei, “Density, Viscosity, and Excess Properties for Aqueous Poly(ethylene glycol) Solutions from (298.15 to 323.15) K,” *J. Chem. Eng. Data*, vol. 53, no. 11, pp. 2598–2601, Nov. 2008.
[35] S. Bicknese, N. Periasamy, S. B. Shohet, and A. S. Verkman, “Cytoplasmic viscosity near the cell plasma membrane: measurement by evanescent field frequency-domain microfluorimetry,” *Biophys. J.*, vol. 65, no. 3, pp. 1272–1282, Sep. 1993.
[36] A. M. Mastro, M. A. Babich, W. D. Taylor, and A. D. Keith, “Diffusion of a small molecule in the cytoplasm of mammalian cells,” *Proc. Natl. Acad. Sci. U. S. A.*, vol. 81, no. 11, pp. 3414–3418, Jun. 1984.
[37] Y. Li, C. Qiao, L. Shi, Q. Jiang, and T. Li, “Viscosity of Collagen Solutions: Influence of Concentration, Temperature, Adsorption, and Role of Intermolecular Interactions,” *J. Macromol. Sci. Part B*, vol. 53, no. 5, pp. 893–901, May 2014.
[38] N. Ziębacz, S. A. Wieczorek, T. Kalwarczyk, M. Fiałkowski, and R. Hołyst, “Crossover regime for the diffusion of nanoparticles in polyethylene glycol solutions: influence of the depletion layer,” *Soft Matter*, vol. 7, no. 16, p. 7181, 2011.
[39] C. M. Schroeder, E. S. G. Shaqfeh, and S. Chu, “Effect of Hydrodynamic Interactions on DNA Dynamics in Extensional Flow: Simulation and Single Molecule Experiment,” *Macromolecules*, vol. 37, no. 24, pp. 9242–9256, Nov. 2004.
[40] J. S. Hur, E. S. G. Shaqfeh, H. P. Babcock, D. E. Smith, and S. Chu, “Dynamics of dilute and semidilute DNA solutions in the start-up of shear flow,” *J. Rheol.*, vol. 45, no. 2, p. 421, 2001.
[41] J. M. Dealy and K. F. Wissbrun, *Melt rheology and its role in plastics processing: theory and applications*. Boston, Mass.: Kluwer Academic, 1999.
[42] L. Sherman, “Novel Rheometer Tells More About Thermoplastic Processing Behavior,” *Plastics Technology*, Sep-2005.

[43] S. Kohl, “Using Rheology to Improve Manufacturing,” *Ceramic Industry*, vol. 152, no. 3, p. 19, Mar-2002.
[44] T. G. Mason, A. Dhople, and D. Wirtz, “Linear Viscoelastic Moduli of Concentrated DNA Solutions,” *Macromolecules*, vol. 31, no. 11, pp. 3600–3603, Jun. 1998.
[45] A. Tsortos, G. Papadakis, and E. Gizeli, “The intrinsic viscosity of linear DNA,” *Biopolymers*, vol. 95, no. 12, pp. 824–832, Dec. 2011.
[46] L. Bravo-Anaya, F. Pignon, F. Martínez, and M. Rinaudo, “Rheological Properties of DNA Molecules in Solution: Molecular Weight and Entanglement Influences,” *Polymers*, vol. 8, no. 8, p. 279, Aug. 2016.
[47] A. Einstein, “<<Eine>> neue Bestimmung der Moleküldimensionen,” 1905.
[48] G. K. Batchelor, *An introduction to fluid dynamics*, 1. Cambridge mathematical ed., 14. print. Cambridge: Cambridge Univ. Press, 2010.
[49] R. B. Bird, W. E. Stewart, and E. N. Lightfoot, *Transport phenomena*, Rev. 2. ed. New York: Wiley, 2007.
[50] T. G. Mason, K. Ganesan, J. H. van Zanten, D. Wirtz, and S. C. Kuo, “Particle Tracking Microrheology of Complex Fluids,” *Phys. Rev. Lett.*, vol. 79, no. 17, pp. 3282–3285, Oct. 1997.
[51] J. Liu *et al.*, “Microrheology Probes Length Scale Dependent Rheology,” *Phys. Rev. Lett.*, vol. 96, no. 11, Mar. 2006.